

**A study of the Flade Isblink ice cap using
a simple ice flow model**

Master Thesis by:

Andreas Lemark

June 2010

Supervisor:

Dorthe Dahl-Jensen

**Niels Bohr Institute
Copenhagen University**



Centre for Ice and Climate



Contents

1	Introduction	1
1.1	The study of ice cores	1
1.2	Flade Isblink	3
1.3	Thesis contents	4
2	Modelling	7
2.1	Theoretical background	7
2.1.1	Deformation of ice	8
2.2	Model	12
2.2.1	Isostatic adjustment	14
2.2.2	Accumulation	17
2.2.3	Numerical solution	17
2.2.4	Dating the ice cap	20
3	Data	25
3.1	Stable Isotopes	25
3.2	ECM	27
3.3	Radar measurements	30
3.4	Melt layers	32
3.5	Temperature measurements	32
3.6	Forcings	33
3.6.1	Mass Balance	33
3.6.2	Temperature	35
4	Application of model	39
4.1	Initial setup	39
5	Results	43
5.1	Age of the ice cap	44
6	Discussion	53
6.1	Applying the time scale to climatic proxies	56
6.2	Discussion of climatic proxies	58
6.3	Future of the ice cap	59
7	Conclusion	61
7.1	Outlook	61
A	Matlab code	I
A.1	Main program	I
A.2	Dating program	III

Abstract

In 2006 an icecore was drilled in north eastern Greenland on the ice cap of Flade Isblink (81.3N, 15.7W) located on the peninsula of Kronprins Christians Land. Harsh weather conditions shortened the time available for drilling, and a total depth of 425 meters was reached, ending the drilling approximately 115 meters above bedrock.

In this thesis a 1D flow model is applied to the buildup of the ice cap, that incorporates the data retrieved from the icecore. The oldest reference point in the ice core is evidence of an eruption by the Icelandic volcano Eldgjá in 934 A.D. found at a depth of 384 meters. Different scenarios are presented, bounding the age of the ice cap between 2800 and 4000 years, most likely nearer the younger value. A climatic study is then done with a time scale acquired from the modelling, showing some of the notable climatic events that have taken place during the past millenium.

Resumé

I år 2006 blev en iskerne boret på iskappen Flade Isblink (81.3N, 15.7W), der befinder sig på halvøen Kronprins Christians Land i nordøst Grønland. Ugunstige vejrforhold betød at der ikke var tid til at bore helt ned til granit, men at boringen måtte stoppe i 425 meters dybde, ca. 115 meter over bunden.

I dette speciale forsøges Flade Isblinks opbygningshistorie at modelleres med en simpel 1D flydemodel. Forskellige kørsler afprøves der inkorporerer data fra iskerneboringen. Det ældste referencepunkt findes i en dybde af 384 meter hvor rester fra den Islandske vulkan Eldgjás udbrud i år 934 findes. Alderen af iskappen fastslås at være et sted mellem 2800 og 4000 år, sandsynligvis nærmere den yngre værdi. Et studie af det seneste årtusindes klimahistorie i området laves herefter med en tidsskala opnået fra modelleringen. Her ses nogle af de klimatiske forandringer der også er velkendte fra andre klimastudier.

1 Introduction

1.1 The study of ice cores

Over the last half century ice cores have proven to be invaluable tools in the study of the paleoclimate. Ice cores drilled on the Greenland and Antarctic Ice Sheets provide a unique insight in the Earth's climate history. The high temporal resolution compared to other climate archives such as deep sea cores and tree rings coupled with the time span of the ice cores provide an unparalleled combination of resolution and time span. In Greenland one can find undisturbed chronologies reaching back over 120.000 years, with annual layer thicknesses of at least 1 cm [NGRIP members 2004].

Through the years, many different branches of climate related glaciology have evolved, as both theoretical and experimental work are required to provide a complete picture of the climatic history. In Greenland, five deep ice cores reaching bedrock have so far been drilled with a sixth (NEEM) in progress. In Figure 1.1 the locations of the drillsites are shown in red. Also shown (in black) are the locations of 3 ice cores drilled on the ice caps along the north and east coast of Greenland. Of these, Flade Isblink will be the particular focus of this thesis.

As ice is a quasi-viscous material it is usual to drill ice cores close to the ice divide. This is where the ice should flow directly down, and chronologies are easiest to interpret here, as there is no horizontal flow of the ice¹. When examining an ice core drilled from an ice cap it is essential to have an accurate dating of the entire length of core, so one can link all other information retrieved from the core to a correct time scale.

¹This only holds true if the location of the summit has not moved over time, but even if this is not the case, it may also be accounted for when interpreting the ice core data.

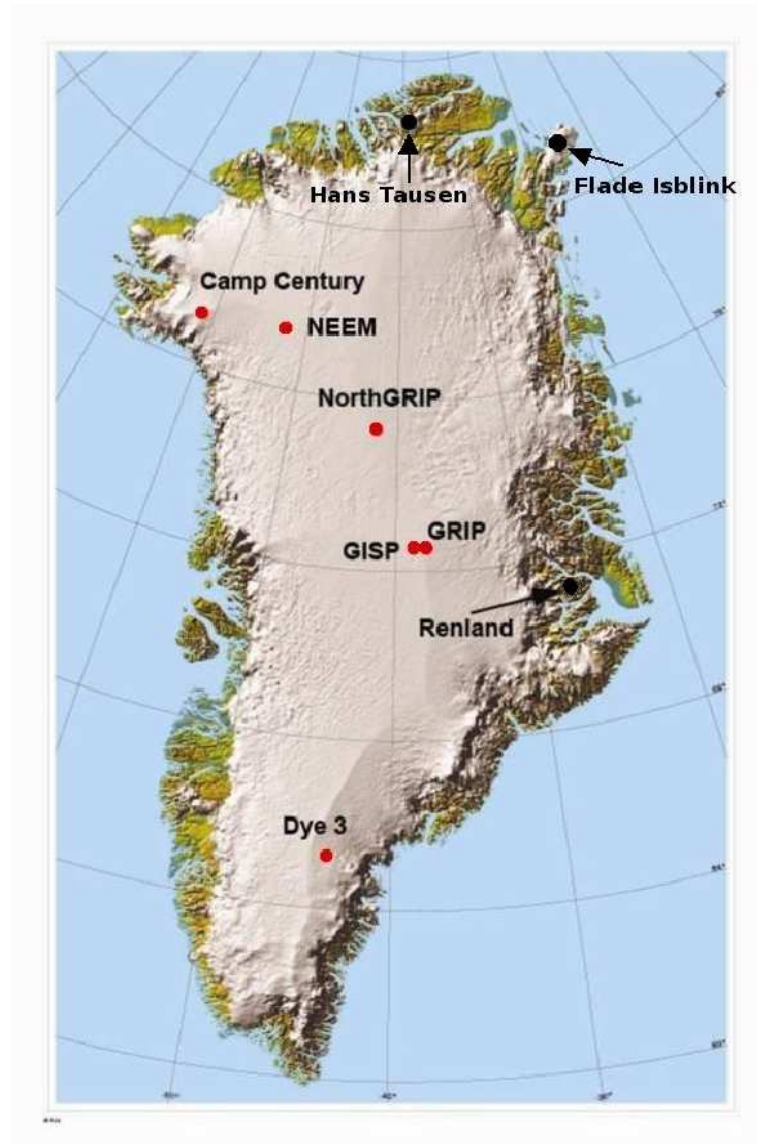


Figure 1.1: Map of Greenland. Red dots indicate deep drill-sites that have reached bedrock or are in progress (NEEM). black dots indicate the three shallow cores drilled in the north-eastern part of Greenland, including Flade Isblink.

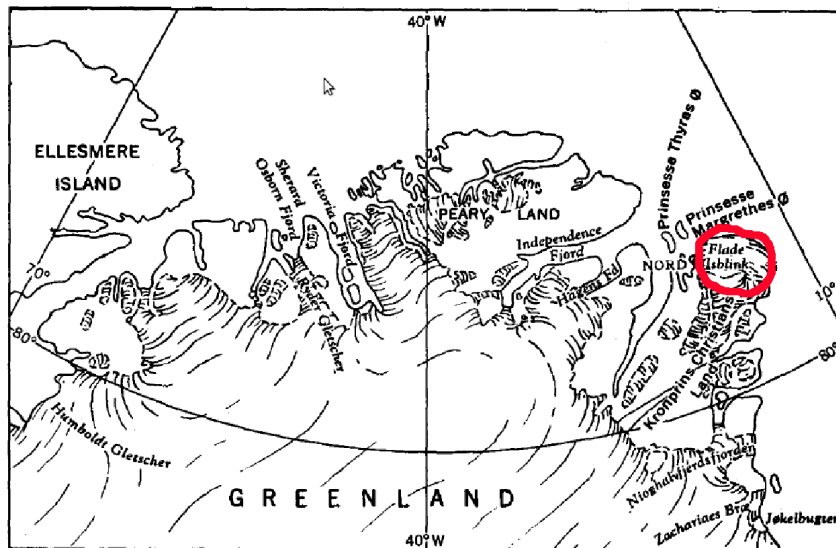


Figure 1.2: Map of northern Greenland. Circled in red is Flade Isblink on the peninsula Kronprins Christians Land .

1.2 Flade Isblink

The ice cap Flade Isblink is located in the furthestmost north eastern corner of Greenland. It is an isolated ice cap with a surface area of 5000 km² extending at most 100 km in the N-S direction and 50 km in the W-E direction. The average height of the underlying bedrock is 100 meters above sea level, and the thickness of the ice reaches approximately 600 m. The ice cap lies on the peninsula Kronprins Christians Land, named after the Danish Crown Prince (later king) Christian the X. It was named and first explored by the polar expedition on Danmarks Ekspeditionen in the early twentieth century. In Figure 1.2 is seen a map of northern Greenland with the ice cap circled in red.

In the summer of 2006, a group led by the Centre for Ice and Climate, Copenhagen University, drilled an ice core at the summit of Flade Isblink 81.2926° N, 15.7029° W. The primary purpose of the expedition was to learn more about the climate in this region of Greenland, and especially the connection to the surrounding sea ice. A total length of 425 meters of ice core was retrieved. Unfortunately bedrock was not reached due to harsh weather conditions reducing the time available for drilling.

Very little is known about the paleoclimate in the north eastern part of Greenland. The few previous studies on shallow ice caps in north east Greenland show the differences in climatic history encountered in this region:

Measurements from an ice core drilled on the Renland ice cap revealed the existence of ice dating back to the previous interglacial, the Eemian, giving it an age of at least 115ky [Johnsen et al. 1992]. In contrast, the ice core retrieved from the Hans Tausen ice cap showed no evidence of even glacial ice. This indicates that the ice cap has grown to existence during the present interglacial period the Holocene. Paleoclimatic records reveal a warm period during the Holocene, where Greenland temperatures were 2–4°C warmer than present [Dahl-Jensen et al. 1998]. This period is known as the Climatic Optimum, and lasted from roughly 8-5 kyr ago. Studies of the Hans Tausen ice cap lead to the conclusion that it is no older than 5 kyr [Madsen 1997, Hammer et al. 2001]. Even though the Hans Tausen and Flade Isblink ice caps are only some hundred kilometers apart, their climatic histories may differ as Flade Isblink is located much lower in altitude, close to the ocean, where the transport pattern of precipitation is likely different. In fact, the very existence of Flade Isblink has been somewhat of a puzzle, as the apparently dry climatic conditions do not at first indicate that the area would sustain an ice cap of Flade Isblinks proportions [Steffensen pers. comm.].

Another goal besides the climatic investigation was to test a new more environmentally friendly drill liquid than previously used. Drill liquid is used below depths of approximately 130 m in ice core drilling. This is due to the large stresses built up in the ice, that may fracture the ice core when it is brought to the surface. The liquid also prevents the ice around the bore hole from deforming and thereby closing the hole. Some criteria are required for the liquid: It must have approximately the same density as the ice, be stable liquid at low temperatures, relatively easy to work with and non-hazardous. The new liquid, based largely on coconut oil, was tested to see what effects it may have on the ice core, how to retrieve the liquid for re-use and generally to learn the properties of it. The new liquid is now in use at the NEEM drill-site.

In this thesis a simple 1D vertically integrated ice flow model is used to investigate the buildup of the ice cap. Preliminary findings from the ice core data indicate that the ice cap did not survive the Climatic Optimum, and has grown to existence at a later time. The buildup history attained from the modelling will be put in a larger context and compared to data from other sources to see what new information may be retrieved about the paleoclimate in this area.

1.3 Thesis contents

The content of this thesis is as follows. In Chapter 2, the theoretical background for ice flow and the physical properties of ice are given, whereafter

the model is presented. Finally the dating method used on the ice cap is explained. In Chapter 3 the data from Flade Isblink and other relevant data are presented. Here the different physical measurements made on the ice core are also explained along with the forcings used to drive the model. The setup of the model as well as different model runs are presented in Chapter 4, and the results and plots are given in Chapter 5. Chapter 6 discusses the different results and tries to tie them to a larger climate history of the area. In Chapter 7 a brief summary of the thesis is given, as well as an outlook on possible further work. In the appendix, section A contains the verbatim source code of the Matlab programme made to compute the results.

2 Modelling

This chapter concerns itself with the theoretical and modelling aspects of the thesis. First there is a discussion of the main concepts and equations related to ice flow. Next the ice flow model is explained along with a simple approach to dating the ice core.

All programming is done in the numerical computing environment, Matlab. The programme used to date the ice core is written by Dorte Dahl Jensen (with minor modifications). Source codes for the programmes used are presented in Appendix A.

2.1 Theoretical background

When fresh snow falls on the ice cap it has a density of 50-70 kg/m³ [Paterson 1994]. Subsequent snowfall compresses the snow until it is transformed into ice by the increasing pressure. Between these two states of snow and glacial ice, there is an intermediate state called firn. The transition from snow to firn is not well defined but after compression by a season of additional precipitation, and a density around 400 kg/m³ the term firn is usually applied. The transition from firn to ice is more sharply defined, as it is the moment of sealing off of the air bubbles in the ice (around 830 kg/m³ [Paterson 1994]), and any further increase in density is solely due to compression of the isolated bubbles in the ice. A maximum density is reached around 917 kg/m³, the exact value depending on pressure, temperature and impurities.

The depth at which the complete transformation from firn to ice takes place depends on accumulation and ice flow. In central Greenland, it is found to

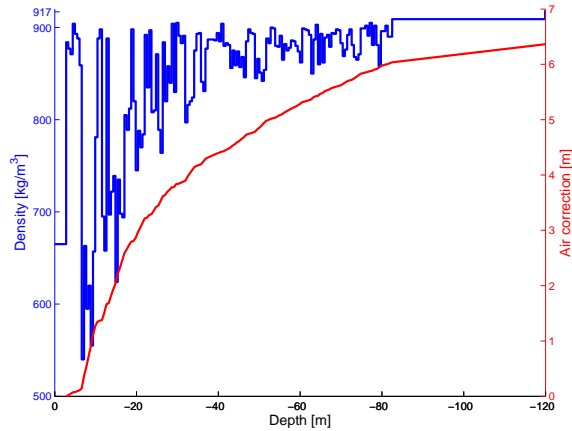


Figure 2.1: The measured density of the ice down through the ice core shown with the air correction. The rapid increases of density in the upper layers and the low value of air correction are an indication of summer melt.

be around 70-100 m [Paterson 1994]. One major influence on the density in the upper layers, is melting during spring and summer. If the temperature rises above the melting point, ice is formed by refreezing of the melted winter snow, rather than by compression of the snow/firn pack.

When working with an ice core, it is customary to use the term ice depth equivalent. This is the depth at which a given layer would be, if all air was removed from the above laying snow and firn, i.e. if the ice cap consisted completely of ice. As with the firn to ice transition, this air correction depends on accumulation, ice flow and temperatures. At Flade Isblink the air column in the ice has been estimated between 6 and 7 meters [Clausen, pers. comm.]. In Figure 2.1 the density profile (blue) of the Flade Isblink ice core is plotted along with the air correction (red). The low value of the air correction compared to central Greenland values around 25 meters is mainly a consequence of the melting and refreezing of summer snow. This in turn leads to complications when modelling the ice cap, discussed in Chapter 2.2.4.

2.1.1 Deformation of ice

The movement of an ice cap is governed by gravity and the flow properties of the ice. The flow properties are in turn governed by values such as accumulation, temperature, impurities and bedrock topography.

As ice is a quasi-viscous material, it will deform either plastically or viscously depending on the strain rate [Budd and Radok 1971, Lautrup 2005]. This expresses itself in the deformation reaction to the stress – when a stress is applied slowly, as in glacial ice flow, the ice deforms permanently, whereas a

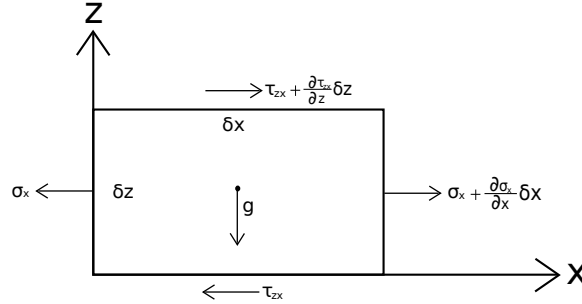


Figure 2.2: Figure showing the stresses acting in the x-direction in a small 2D block of ice with sides δx and δz .

rapid increase of stress will tend to break the ice¹. Acceleration terms may be neglected due to the slow velocity of the ice flow, and looking at a small block of ice embedded in the ice cap, the governing equations of the ice flow show the relation between forces acting on the *surface* of the block and the (gravitational) force acting on the *entire* block [Budd and Radok 1971]:

$$\begin{aligned}
 \frac{\partial \delta_x}{\partial x} + \frac{\partial \tau_{xy}}{\partial y} + \frac{\partial \tau_{xz}}{\partial z} &= 0 \\
 \frac{\partial \delta_y}{\partial y} + \frac{\partial \tau_{yx}}{\partial x} + \frac{\partial \tau_{yz}}{\partial z} &= 0 \\
 \frac{\partial \delta_z}{\partial z} + \frac{\partial \tau_{zx}}{\partial x} + \frac{\partial \tau_{zy}}{\partial y} &= -\rho g
 \end{aligned} \tag{2.1}$$

Here presented in a cartesian coordinate system with z pointing up from the bed and x and y in the plane. With δ denoting normal stresses, τ denoting shear stresses and subscripts indicate the directions of the surface and the force, respectively. ρ is the density of the ice and g the gravitational acceleration. The above notations will be used throughout the chapter. Some simplifying assumptions are also made in this work: the ice is assumed isothermal, hence no temperature gradients are calculated. The flow is assumed only in the x, z plane so that all terms containing y disappear, and the ice is assumed to be isentropic. In Figure 2.2 the stresses acting on a two dimensional block of ice are shown.

The ice is taken as incompressible, and from the continuity equation in a two dimensional form we get

$$\frac{\partial u}{\partial x} + \frac{\partial w}{\partial z} = 0 \Leftrightarrow \frac{\partial w}{\partial z} = -\frac{\partial u}{\partial x} \tag{2.2}$$

¹A fact utilized when retrieving drilled ice cores.

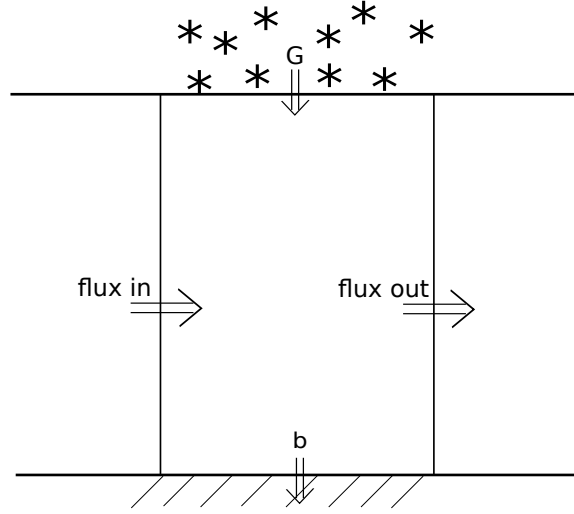


Figure 2.3: The change of ice thickness depends on the fluxes through the ice section. If the height is constant, the fluxes balance out due to conservation of mass.

From the conservation of mass we then have that all fluxes through a section of ice must cancel out. This is shown in Figure 2.3, where G and b are the mass balance at the top and bottom of the section, respectively. From the figure we also see that the change of ice thickness, H relates to the horizontal velocity by

$$\frac{\partial H}{\partial t} = G + b - \frac{\partial q_x}{\partial x} \quad (2.3)$$

Where q_x is the mass flux, $q_x = H(x) \cdot \bar{u}$. The mean horizontal velocity is defined as $\bar{u} = \frac{1}{H} \int_0^H u dz$. Assuming no basal melt ($b = 0$), Equation 2.3 may then be written as

$$\frac{\partial H}{\partial t} = -\frac{\partial}{\partial x} \left(\int_0^{\text{surface}} u dz \right) + G \quad (2.4)$$

Laboratory studies on the strain rates of ice have given some empirical relations useable for modelling work. For an interval of stresses related to glacial ice flow, one relation between the strain rate and stresses is:

$$\dot{\epsilon} = \mathbb{A} \tau_{xy}^n \quad (2.5)$$

Where $\dot{\epsilon}$ is the vertical strain rate and τ_{xy} is the effective shear stress, n is a constant, while the value of \mathbb{A} is temperature dependent. This relationship

is sometimes known as *Glen's Law*, although strictly speaking it is based on empirical observations [Glen 1955]. The shear stress τ is a function of the *deviatoric stresses*, i.e. the deviations from hydrostatic equilibrium. Since the ice is assumed incompressible, the deviatoric stresses are often used to describe the deformation of the ice¹. The value of the constant n is not well-defined, but most studies show satisfactory results with $n = 3$, though it is proposed that the value of n rises when stresses grow larger, and larger values have been related to microcracks in the ice [Petrenko and Whitworth 1999]. A value of $n = 1$ indicates a totally viscous (liquid) material whereas $n = \infty$ yields a perfectly plastic material – in this regard the value of n illustrates the quasi-viscous properties of ice. The value of \mathbb{A} follows the Arrhenius relation:

$$\mathbb{A} = A_0 \exp(-Q/RT) \quad (2.6)$$

Where A_0 is a constant, $R = 8.314 \text{ J}/(\text{mol}\cdot\text{K})$ is the molecular constant, Q is the activation energy for creep-flow and T is the temperature. Since the value of \mathbb{A} is temperature dependent and relates to the flow velocity of the ice, this may physically be interpreted as the ice 'softening' with higher temperature.

The flow law presented in Equation 2.5 does not take into account that the ice is anisotropic, as later more advanced equations do (e.g. [Azuma 1994]). In this thesis the calculations relating to anisotropies would be too complex, and the ice is assumed isotropic.

Following [Weertman 1961] we now assume perfect plasticity of the ice. Here we assume all shear stresses occur near the bottom of the ice and a mechanical equilibrium may be reached, where the bottom stress is balanced by the gravitational pull on the ice. This bottom stress is sometimes called the *yield stress* and as stresses build up in the ice cap the basal stress will reach and never exceed this value. Figure 2.4 shows a scenario for a square block of ice frozen to bedrock with a small slope α , but the following deduction may also be shown to apply for ice resting on a flat bed, with the surface slope of the ice being α [Paterson 1994].

If we assume the ice does not slide, the bottom stress τ_b is balanced by the gravitational effect. A value of τ_b between 50-150 kPa is often found appropriate depending on the size of and impurities in the ice cap. Calling the surface slope $\frac{dH}{dx}$, this leads to the equation

$$\tau_b = \rho g H \frac{dH}{dx} \quad (2.7)$$

¹see [Paterson 1994] for an elaboration.

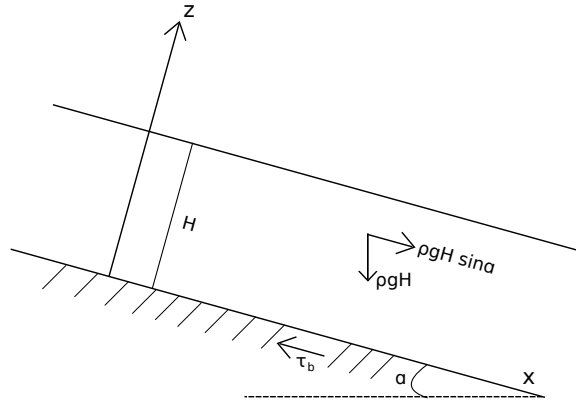


Figure 2.4: Assuming all shear stress occurs near the bottom, the stresses balanced in an ice cap in mechanical equilibrium.

It is assumed that the slope is relatively small and the length and width are large compared to the thickness of the ice. The assumption of perfect plasticity and hence a dominating bottom shear stress is not valid at the ice divide since longitudinal stresses become important here. Likewise, at the ice margin where the shear stresses tend to zero, the assumption breaks down.

From Equation 2.7 we have a first order approximation of the relation between the thickness and horizontal dimensions of an ice cap. Isolating H in Equation 2.7 produces a parabolic shape and it is also seen that the value of $H \frac{dH}{dx}$ is constant. The assumption of perfect plasticity leads to modelled results that are in good agreement with observed surface profiles of ice caps.

The above considerations give all the tools for making a simple flow model of an ice cap of the right proportions. This shall be dealt with in the following part.

2.2 Model

The main model used in this thesis is a simple 1D model based on the works of Oerlemans [Oerlemans 1981, Oerlemans 1980]. The ice cap is vertically integrated, calculating the ice flow from changes in the height driven by internal stresses and accumulation history. It assumes a simple flow law, relating to the vertically integrated mean velocity and bottom shear

$$\bar{u} = B\tau_b^m \quad (2.8)$$

Where \bar{u} is the mean horizontal velocity, and τ_b is taken from Equation

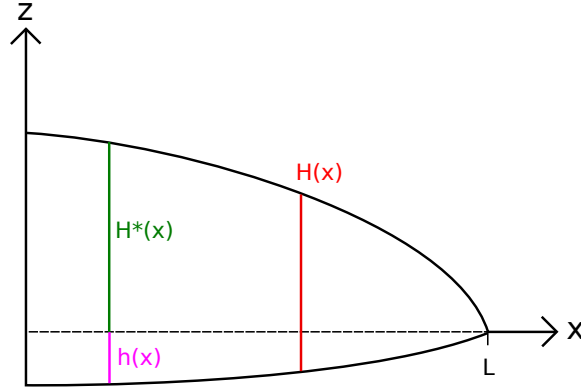


Figure 2.5: The coordinate system applied in this work. The horizontal coordinate x , is zero at the ice divide while the vertical coordinate z , is positive above sealevel. The thickness of the ice is $H(x)$, while the surface of the bedrock is found at height $h(x)$. The value $H^*(x)$ is the height of the ice surface above sealevel, while the ice extends a length of L from the ice divide.

2.7. The value of B is temperature dependent, but as the ice is assumed isothermal in this work, it is taken as constant. The constant m depends on the amount of basal sliding contributing to the velocity but the value lies somewhere between 2 and 3 [Oerlemans 1981].

Figure 2.5 shows the coordinate system used in the model. The horizontal coordinate x , is zero at the ice divide while the vertical coordinate z , is positive above sea level. The thickness of the ice is $H(x)$, while the surface of the bedrock is found at height $h(x)$. The value $H^*(x)$ is the surface of the ice, and is defined by $H^*(x) = H(x) + h(x)$. The total extent from the ice divide is labeled L .

The vertically integrated flow may then be found from Equations 2.7 and 2.8, noting that in Equation 2.7 the surface change with distance relates to H^* , not H .

$$q_x = H\bar{u} = AH^{m+1} \left(\frac{\partial H^*}{\partial x} \right)^m \quad (2.9)$$

Where A is a constant incorporating g, ρ and B . Inserting the above value of q_x in Equation 2.3 produces

$$\frac{\partial H}{\partial t} = \frac{\partial}{\partial x} \left(AH^{m+1} \left(\frac{\partial H^*}{\partial x} \right)^m \right) + G \quad (2.10)$$

Where G is the accumulation in meters of ice equivalent, and we assume no basal melt. We now regard the flow as a diffusive process, where ice flows

from accumulation zones to ablation zones, writing Equation 2.10 as

$$\frac{\partial H}{\partial t} = \frac{\partial}{\partial x} \left(D \frac{\partial H^*}{\partial x} \right) + G \quad (2.11)$$

Where the diffusivity, D is given by

$$D = AH^{m+1} \left(\frac{\partial H^*}{\partial x} \right)^{m-1} \quad (2.12)$$

As mentioned in Chapter 2.1 the assumptions leading to Equation 2.7 do not apply at the ice divide and margin, and Equation 2.11 represents a mean over the entire ice cap, as do the values of A and m . The constants A and m are crucial to the relationship between the height/width and the slope at the margin, respectively. As one of the boundaries of the model is the appearance and extent of the ice cap, the value of these two parameters may help producing an ice cap of the right proportions. In this work they are set to $A = 0.1$ and $m = 2$.

2.2.1 Isostatic adjustment

Due to the viscous properties of the Earth's mantle, it will deform when a sufficiently large load (such as an ice cap) is added to the crust, leading the crust to sink under the applied weight – this is known as isostatic adjustment, and is seen in Figure 2.6.

Isostatic depressions from large loads, such as the Greenland Ice Sheet may be approximated by balancing the weight of the ice with that of the depressed crust. A typical density for the continental crust is 2700 kg/m^3 [Skinner and Porter 1987]. After an equilibrium is reached, an ice cap with a density of 917 kg/m^3 will infer an isostatic depression approximately $1/3$ of the height, H . Therefore [Oerlemans 1981] applied the following equation for the bedrock change of height with time

$$\frac{\partial h}{\partial t} = -\alpha(H + 3(h + h_0)) \quad (2.13)$$

Where h_0 is the height of the bedrock if no ice cap was present and $\frac{1}{2\alpha}$ is the time it takes to reach a full depression. An ice cap of Flade Isblinks dimensions will not infer a full isostatic depression though, but rather be scaled by a factor of .5 due to the localized concentration of the load [Brotchie and Silvester 1969]. This means that a new equilibrium would be reached after a depression of $1/6$ of the height. The timescale for a complete

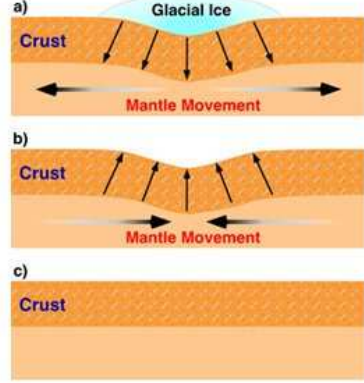


Figure 2.6: Sketch of the isostatic response and adjustment of the crust and mantle to an applied load. Figure taken from <http://www.physicalgeography.net/>

isostatic adjustment is about $T_{iso} = 1000$ years [Dahl-Jensen, pers. comm.], setting the value of α in Equation 2.13 to $\alpha = \frac{1}{T_{iso}} = 5 \cdot 10^{-4} \text{ y}^{-1}$.

There is evidence that during the last glacial period the peninsula of Kronprins Christian Land was covered by ice connected to the main Greenland Ice Sheet [Funder and Hansen 1996], which means that the area around Flade Isblink has gone through an uplift during the Holocene, as a reaction to the depression experienced under the former ice sheet. Figure 2.7 taken from [Funder and Hansen 1996] shows the calculated relative change in height above sea level of the Greenland coast since the last glacial retreat. They evaluate approximately 40-80 meters of sea level change at Kronprins Christian Land since the end of the last glacial. The uplift is thought mainly to have occurred after the rapid decay of the overlaying ice approximately 10 kyr ago. This adds a term to the uplift from the previous ice masses, and the final appearance of the isostatic equation then becomes

$$\frac{\partial h}{\partial t} = -\frac{1}{2000} (H + 6(h - h_0)) + \frac{dh_0}{dt} \quad (2.14)$$

Where $\frac{dh_0}{dt} = \frac{40\text{m}}{10000\text{y}} = 4 \cdot 10^{-3} \text{ m/y}$ is taken from the minimum evaluated uplift in the area over the last 10 kyr. The added term implies that the bedrock may be rising, even though it is ice covered.

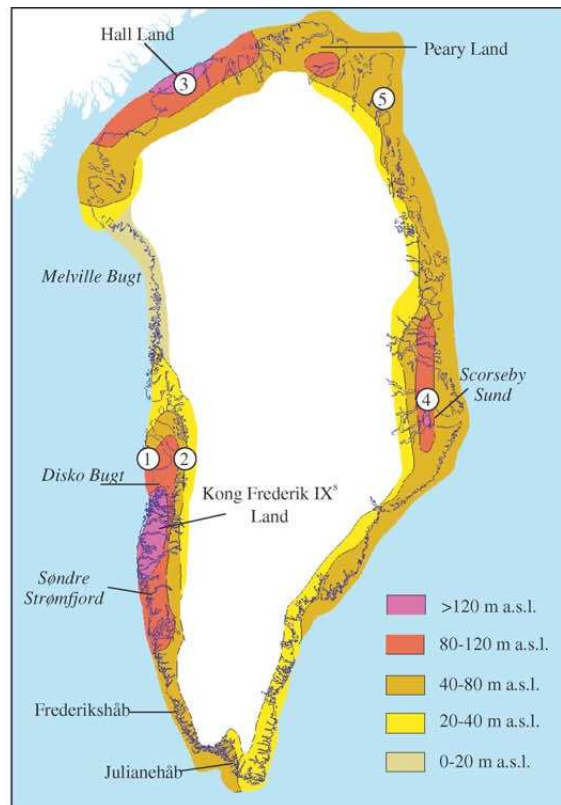


Figure 2.7: The estimated isostatic response from marine evidence, since the last glacial period. Kronprins Christian Land with Flade Isblink is found in area (5) with a change of height above sealevel estimated between 40-80 meters since the rapid decay of the overlying ice approximately 10 kyr ago. Figure taken from [Funder and Hansen 1996].

2.2.2 Accumulation

The final parameter needed for the modelling is how the mass balance is calculated. The mass balance curve used in [Oerlemans 1981] is derived from a second degree polynomial, with the variable being the surface height above the equilibrium line ($H^* - E$), where E is the position of the equilibrium line. The equilibrium line is defined as the height at which the mass balance rate is zero, and the mass balance rate is defined as the annual gain¹ of mass at the ice cap surface [Oerlemans 2008].

The appearance of the mass balance curve is highly dependent on the location of the ice cap and climatic conditions in the area. A maritime ice cap near sea level will typically have a stronger mass balance dependence on height, than the dry, high-altitude central Greenland Ice Sheet [Oerlemans 2008, Paterson 1994]. Also the mass balance will not continue to rise with height but reach a maximum value at some height, H_{max} above E . Above H_{max} the mass balance will decrease slightly with height. The physical interpretation of this maximum is that less moisture will be able to reach the central parts of the ice cap if the ice cap is sufficiently large [Boulton et al. 1984]. The mass balance applied in this work is not identical to that in [Oerlemans 1981], but is still a function of the surface height above E . Constraints on the mass balance are based on radar images and estimates of annual layer depths back in time. Within these constraints, the exact appearance of the curve may be varied during different model runs. In Chapter 3.6 the mass balance applied in this work will be discussed further.

The model is completely specified by Equations 2.11-2.14, a given mass balance curve and the requirement that $H \geq 0$.

2.2.3 Numerical solution

The Equation 2.11 is solved numerically using finite differences on a staggered grid, with Δx being the spatial step and the distance, x discretized as

$$x_i = i\Delta x, \quad i = [0, 1, 2, \dots, N - 1]$$

over the domain $0 \leq x \leq L_x$. With $L_x = \Delta x(N - 1)$.

The discretization of the right-hand side of Equation 2.11 then becomes

¹a negative mass balance means an annual loss

$$\frac{\partial H}{\partial t} = \frac{\overbrace{D_{i+\frac{1}{2}} - D_{i-\frac{1}{2}}}^{\frac{\partial D}{\partial x}|_i}}{dx} \frac{\overbrace{H_{i+1} - H_{i-1}}^{\frac{\partial H}{\partial x}|_i}}{2dx} + D_i \frac{\overbrace{H_{i+1} - 2H_i + H_{i-1}}^{\frac{\partial^2 H}{\partial x^2}|_i}}{dx^2} + G_i \quad (2.15)$$

With the discretization of the diffusion being:

$$\begin{aligned} D_i &= AH_i^{m+1} \left(\frac{H_{i+1}^* - H_{i-1}^*}{2\Delta x} \right)^{m-1} \\ D_{i+\frac{1}{2}} &= A \left(\frac{H_{i+1} + H_i}{2} \right)^{m+1} \left(\frac{H_{i+1}^* - H_i^*}{\Delta x} \right)^{m-1} \\ D_{i-\frac{1}{2}} &= A \left(\frac{H_i + H_{i-1}}{2} \right)^{m+1} \left(\frac{H_i^* - H_{i-1}^*}{\Delta x} \right)^{m-1} \end{aligned}$$

Equation 2.12 leads to the diffusion being zero at the terminus and summit, since H and $\frac{dH^*}{dx} = 0$ here, respectively. To circumvent this in the numerical calculations, a minimum value, D_0 is included, with a value approximately two orders of magnitude lower than typical diffusion values. Sensitivity measurements by [Oerlemans 1981] indicate that the exact value of D_0 is not significant for the final results. The values of D and G depend (indirectly) on the height of the bedrock. Equation 2.14 is therefore also discretized as

$$h^{j+1} = h^j - \alpha \Delta t (H^j + 12(h^j - h_0^j)) + \left(\frac{h_0^{j+1} - h_0^j}{\Delta t} \right) \Delta t \quad (2.16)$$

Where superscript j indicates the discrete timestep and Δt is the size of the timestep.

The method applied to discretize the left hand side of Equation 2.15, is a Crank-Nicolson scheme. The Crank-Nicolson scheme is a finite-difference method for solving partial differential equations, utilising the forward Euler and backward Euler method in time. A partial differential equation of the form $\frac{\partial u}{\partial t} = F(u, x, t, \frac{\partial u}{\partial x}, \frac{\partial^2 u}{\partial x^2})$ leads to the Crank-Nicolson solution

$$\frac{u_i^{j+1} - u_i^j}{\Delta t} = \frac{1}{2} [F_x(i, j) + F_x(i, j+1)] \quad (2.17)$$

Where i and j indicate the discrete spatial and time steps respectively and F^j and F^{j+1} , the forward and backwards Euler solution respectively [Press et al. 2003].

The Crank-Nicolson method is *implicit*, where the evolution relies on both the current value and the value at the following timestep. Therefore it is simplified by in each iteration setting

Where the letters $a - f$ indicate the values related to the distinct spatial- and time steps in Equation 2.20. The vector \bar{H}^{j+1} may be isolated as

$$\underline{\underline{A}}\bar{H}^{j+1} = \underline{\underline{B}}\bar{H}^j + \bar{C} \Rightarrow \bar{H}^{j+1} = \underline{\underline{A}}^{-1}(\underline{\underline{B}}\bar{H}^j + \bar{C}) \quad (2.21)$$

Represented here in a more compact form, where the double underline indicates a matrix. The boundary conditions are implemented in the following way: at the ice divide the symmetry of the ice cap is utilized, so only points within the grid are applied, likewise at the terminus, the height of the bedrock, h , is used as H^* for the final spatial step. Due to the implementation of a minimum value D_0 , the values D_2 and D_{N-2} are found by interpolation of the other values of D . This is purely for technical reasons and should not influence the final model.

The model is run with a spatial resolution of one kilometer and temporal resolution of one year – that is $\Delta x = 1$ km, $\Delta t = 1$ year.

2.2.4 Dating the ice cap

To relate the climatic changes represented by proxy data in an ice core it is essential to have an accurate dating of the entire core. When possible, a combination of many methods is used to produce a consecutive chronology. Analyses on stable isotopes ($\delta^{18}\text{O}$ and δD), chemical impurities, conductive properties, gas content and visual stratigraphy may all be used towards dating the ice core. Applying many different dating tools heightens the likelihood of getting an accurate chronology, and discovering anomalies or miscalculations in one or more of the methods. Also the different methods may not all be optimal for the entire core length, depending on climatic conditions at the time of deposition through the ice core.

As the ice travels down through the ice cap it experiences both vertical compression and longitudinal stresses from the ice flow. Therefore annual layers will thin towards the bottom and in deep drilled ice cores deteriorating resolution will eventually make counting annual layers an unfeasible approach. Even so, in this way the NGRIP ice core has been dated back 60 kyr with a combination of the above mentioned methods [Svensson et al. 2008].

An important supplement to these *stratigraphic* methods is computerized modelling of the ice flow, where the age of a given layer is calculated using some simplifying assumptions. The constraints in these models may be fixpoints of parameters such as age and past accumulation rates that in turn may be acquired from the stratigraphic analyses [Hammer et al. 1978]. In the following, some simple flow models are presented.

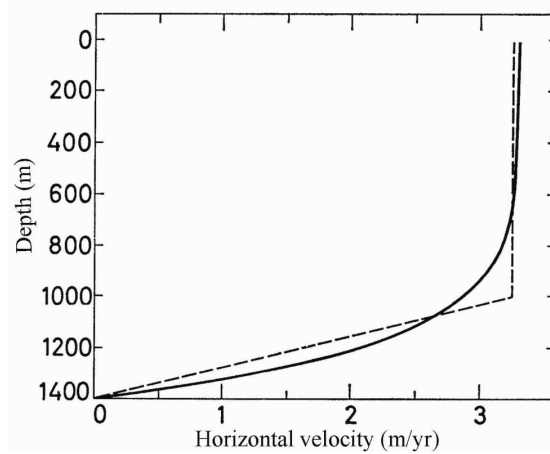


Figure 2.8: The dashed line shows the horizontal flow in the Dansgaard-Johnsen model. The horizontal velocity is constant down to a certain height, and then decreases linearly towards the bottom. This produces a kink in the graph at height h , leading to the nickname 'kink model'. The solid line shows the flow velocities calculated using Glen's Law. Figure taken from [Dansgaard and Johnsen 1969].

The horizontal velocities are almost constant down through an ice cap, only changing noticeably near the base where deformation is mostly due to shear. Nye therefore made the simplifying assumption that the vertical strain rate down through a vertical column is constant, leading to a constant horizontal velocity down through the ice cap [Nye 1957]. This gives a good first-order estimate of the flow in the top layers, but as the strainrate $\dot{\epsilon} = 0$ at the bottom¹, the shortcomings of the Nye model become evident when modelling the lower layers of an ice cap.

The Dansgaard-Johnsen (D-J) model is also simple, but greatly improves the Nye model by allowing the vertical strain rate (and thereby the horizontal velocity) to change down through the ice cap [Dansgaard and Johnsen 1969]. In Figure 2.8 is seen the horizontal velocity applied in this model – also shown in the figure is the velocity down through the ice when calculating the flow using Equation 2.5. Comparing the D-J model to the velocity acquired from Glen's law, it is seen that the simple approximation of the D-J model is in fact quite good – bearing in mind that Glen's law itself is an approximation².

¹assuming the ice is below the pressure melting point

²Glen's law does not take into account the deformation history of the ice, and is only applicable to the 'secondary creep' phase of the ice flow.

The flow in the D-J model is expressed by the following equation

$$u(x, z) = u_{sur}(x) \cdot \begin{cases} 1 & z \in [h_k, H[\\ F_B + (1 - F_B)\frac{z}{h_k} & z \in [0, h_k[\end{cases} \quad (2.22)$$

Where u_{sur} is the horizontal surface velocity. Equation 2.22 simply states that the horizontal velocity u is constant down to some given height, h_k ¹ below which it decreases linearly to a fraction of the surface velocity, F_B .

In its original form, the D-J model assumes a history of constant accumulation, as does the Nye model. This is rarely the case, and improvements have been made in estimating past accumulation rates, by assuming a relation between these and stable isotope values [Dahl-Jensen et al. 1993].

Inserting Equation 2.22 into Equation 2.4 and performing the integration leads to

$$\frac{\partial H}{\partial t} = -\frac{\partial u_{sur}}{\partial x} \left(H - \frac{h}{2}(1 - F_B) \right) + a \quad (2.23)$$

And after rearranging, we get the change in surface velocity with distance

$$\frac{\partial u_{sur}}{\partial x} = \frac{a - \frac{\partial H}{\partial t}}{H - \frac{h}{2}(1 - F_B)} \quad (2.24)$$

From the continuity Equation 2.2 and Equation 2.22, it is possible to isolate the vertical velocity, w and performing the integration leads to the result

$$w = -\frac{\partial u_{sur}}{\partial x} \cdot \begin{cases} z - \frac{h_k}{2}(1 - F_B) & z \in [h_k, H[\\ \frac{1}{2}(1 - F_B)\frac{z^2}{h_k} + F_B z & z \in [0, h_k[\end{cases} \quad (2.25)$$

From w it is now possible to trace the movement of a particle in time. Since $w \equiv \frac{\partial z}{\partial t}$, we can calculate the new position, z_2 at time t_2 of a particle originating from z_1 at time t_1 , by insertion in the following equation

$$\int_{t_1}^{t_2} dt = \int_{z_1}^{z_2} \frac{dz}{w}$$

Depending on the position of z_1 the integral on the right-hand side of this equation takes different forms. First, we look at a point originating **above** h_k

¹The subscript, k is short for kink due to the nickname mentioned earlier.

$$\Delta t = -\frac{\partial u_{sur}}{\partial x} \int_{z_1}^{z_2} \frac{dz}{z - \frac{h_k}{2}(1 - F_B)} \quad (2.26)$$

Where we call $\Delta t = t_2 - t_1$. The new position, z_2 may then be isolated to produce:

$$z_2 = \left(z_1 - \frac{h_k}{2}(1 - F_B)\right) \exp\left(-\Delta t \frac{\partial u_{sur}}{\partial x}\right) + \frac{h_k}{2}(1 - F_B) \quad z_1 > h_k \quad (2.27)$$

Where $\frac{\partial u_{sur}}{\partial x}$ is given by Equation 2.24.

If the particle originates **below** h_k , then the integral takes the form:

$$\Delta t = -\frac{\partial u_{sur}}{\partial x} \int_{z_1}^{z_2} \frac{dz}{F_B z - \frac{1}{2h_k}(1 - F_B)z^2} \quad (2.28)$$

And the new position is again found by integration:

$$z_2 = \frac{F_B C}{1 - \frac{1}{2h_k}(1 - F_B)C} \quad z_1 < h_k \quad (2.29)$$

Where

$$C = \frac{z_1}{F_B + \frac{1}{2h_k}(1 - F_B)z_1} \exp\left(-\Delta t F_B \frac{\partial u_{sur}}{\partial x}\right)$$

In the above calculations $\frac{\partial u_{sur}}{\partial x}$ has been taken as constant during each integration step. Since the model is run with a temporal resolution of $\Delta t = 1$ year, this should not affect the final result significantly. Furthermore, it should also be tested whether a layer passes the kink height h_k during the integration. If it does, z_2 in Equation 2.27 should be found by using Equation 2.26 down to the kink height and Equation 2.28 below it, but sensitivity runs of the programme where this is taken into consideration, produce similar results to runs without. As the depth of the kink height itself is just a rough estimate, this will probably be a larger source of uncertainty, than the error from these approximations. Using a $\Delta t = 1$ year also means that the annual layer thickness, λ , at a specific depth in the ice cap may be found simply by subtracting two subsequent calculated layer depths from each other.

The input for the programme calculating the depth-age relation are the parameters acquired from the modelling of the build-up of the ice cap. The

values of the D-J model parameters are set to $h_k = 0.2H$ and $F_B = 0.1$. A value of $h_k \approx \frac{1}{3}H$ is often used for modelling the central Greenland Ice Sheet. In a relatively warm ice cap like Flade Isblink, with ragged bedrock topography the bottom shear will be more dominating, leading to the lower set value of h .

3 Data

In this chapter the data used in the modelling of the ice cap is examined. First presented are the measurements made on the Flade Isblink ice core along with other direct measurements from the ice cap and surrounding area. Next the forcings used to drive the model are introduced. A total of 425 meters of ice core was retrieved, ending approximately 115 meters above bedrock.

3.1 Stable Isotopes

By far the most common oxygen isotope found in natural H_2O is ^{16}O . A small fraction ($\approx 2\%$) consists of the heavier oxygen isotope ^{18}O [Paterson 1994]. Since the vapour pressure for the heavier isotope is lower, a fractionation occurs during evaporation and condensation. The amount of fractionation is temperature sensitive, which means that differences in the isotope ratios are related to the temperature at the time of deposition [Dansgaard 1964]. Assuming temperatures in the source area remain constant, the concentrations may be used as a proxy for past temperature variations in the precipitation area. The measure of this variation is called the $\delta^{18}\text{O}$ value¹. It is defined as the relative deviation from a standard sample², and found by the following equation

$$\delta^{18}\text{O} = \frac{R_{\text{sample}} - R_{\text{VSMOW}}}{R_{\text{VSMOW}}}, \quad R = \frac{[^{18}\text{O}]}{[^{16}\text{O}]} \quad (3.1)$$

Where R_{sample} is the ratio in the sample and R_{VSMOW} is the standard value. The relative deviation is used, as the deviations from the standard are often

¹pronounced delta - O - eighteen.

²Usually the Vienna Standard Mean Ocean Water (VSMOW) is used.

small and they are easier to measure than the absolute deviations. It is also common to present $\delta^{18}\text{O}$ values in ‰ (per mil). Note that in ice cores the $\delta^{18}\text{O}$ values will be negative as the fractionation favours higher concentrations of the lighter ^{16}O isotopes.

As clear annual variations are often seen in the $\delta^{18}\text{O}$ signal, it is common to use the record both for dating ice cores and as a climate indicator. By correlating measured values of $\delta^{18}\text{O}$ and temperature from many different sampling stations a linear relationship is found of approximately $1.5^\circ\text{C}/\text{‰}$ [Dansgaard 1964, Johnsen et al. 1995]. This relationship represents a spatial not temporal distribution however, and the relationship between $\delta^{18}\text{O}$ and temperature have most likely changed both regionally and in time, due to changes in precipitation patterns, climate or other, unknown factors.

The independent paleotemperature measurements obtained from inversions of borehole temperatures may give a temporal relation between $\delta^{18}\text{O}$ and temperature variations¹. Data from the GRIP ice core reveal temperatures during the Last Glacial Maximum (the coldest period of the previous glacial) that are $23 \pm 2^\circ\text{C}$ lower than at the time of measuring. Meanwhile GRIP $\delta^{18}\text{O}$ values from the same period show values 7-8 ‰ lower than present [Johnsen et al. 1997]. This relation back in time shows a correlation of approximately $3^\circ\text{C}/\text{‰}$ during LGM or about twice that of the present values.

Despite the uncertainties and assumptions related to the interpretations of $\delta^{18}\text{O}$ measurements, the use of stable oxygen isotope ratios as proxy for temperature is one of the most fundamental relationships used in climatic glaciology.

The $\delta^{18}\text{O}$ measurements are carried out at the Centre for Ice and Climate in Copenhagen. The ice core is melted and brought in contact with gaseous carbon dioxide (CO_2), until the gas reaches an isotopic equilibrium with the melted ice. The gas is then sent through a mass spectrometer to measure the isotopic oxygen ratio. The top 290 meters were sampled in 2.5 cm segments, while the lowest 155 meters were measured with a coarser resolution of 55cm. In principle this should give a resolution of 2.5 cm for the top 290 meters, but large parts of the ice core have suffered melting, mixing the precipitational layers. Percolation and refreezing will tend to disturb or even obliterate the continuous $\delta^{18}\text{O}$ signal and resolution is therefore lowered considerably. Since the annual resolution is lost the $\delta^{18}\text{O}$ signal cannot be used as a dating marker, but large-scale variations may still be preserved in the signal. In Figure 3.1 the $\delta^{18}\text{O}$ values down through the ice core is shown. Also plotted are the smoothed values using a 300 datapoint running mean average.

¹These measurements will be elaborated on in Chapter 3.6.2.

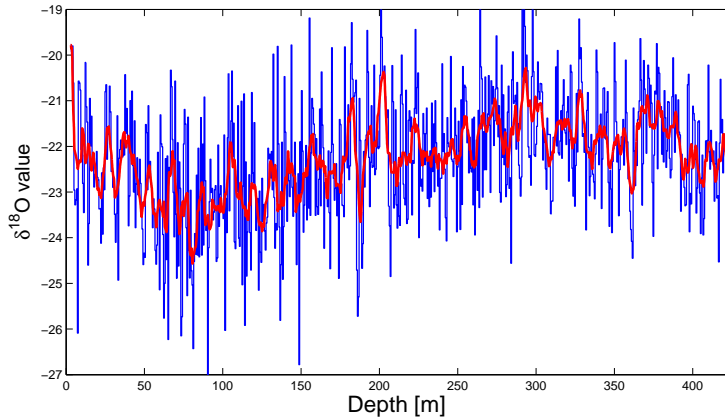


Figure 3.1: Plot of the parameter $\delta^{18}\text{O}$ down through the ice core.

3.2 ECM

The Electrical Conductivity Measurement (ECM) is a method of easily and effectively measuring the acid/base balance down through an ice core [Hammer 1980]. It is most often done directly in the field for practical purposes and as it is a non-destructive measurement. Measuring ECM consists of taking two electrodes with a potential of ≈ 1000 V between them, and at an adequate pace¹ sliding them down the clean-cut surface of the ice core. Figure 3.2 shows the basic outline of the ECM setup.

The idea behind ECM is the correlation between the acidity of the ice and its electrical conductivity. Measurements of H_3O^+ (pH-values) on melted samples are related to electrical measurement on the ice, and the acid concentrations are found from the relation:

$$\text{H}^+ = 0.045i^{1.73} \quad (3.2)$$

Where i is the current (in μA) and H^+ is the acid concentration.

The measurements display both annual signals and sharp peaks in acidity concentrations due to volcanic activity. During volcanic outbursts, large amounts of gases such as sulphur dioxide (SO_2) are flung high into the atmosphere. In the atmosphere the sulphur dioxide combines with water (H_2O) to produce sulphuric acid (H_2SO_4), and when it reaches the ice cap, may be detected in the ECM signal by sharp rises in the H^+ value [Hammer 1980]. The seasonal variations may be due to several factors. During spring and summer large amounts of hydrogen sulphide (H_2S) are introduced to the

¹Fast enough to prevent strong polarization, yet also slow enough to get a continuous record.

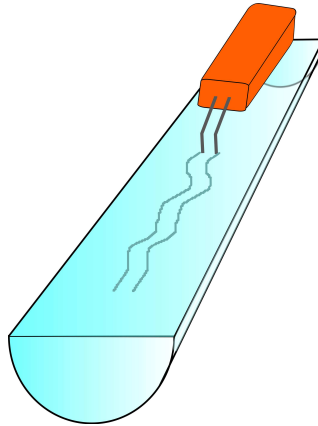


Figure 3.2: Setup of the Electrical Conductivity Measurements performed on an ice core – two electrodes are slid along the prepared ice core surface, with a potential of ≈ 1000 V between them, thereby registering the electrical conductivity of the ice.

atmosphere, here being oxidized to produce sulphuric acid [Hammer 1980]. Chemical impurities such as nitrate and sulphate ions raise the acid concentrations while alkaline dust and ammonium (NH_4^+) lowers it – and all these parameters show seasonal variations [Steffensen 1988, Meese et al. 1997].

The ECM method is quite sensitive to temperature values, both at time of deposition and measurement, which may be very influential on the Flade Isblink data. When summer temperatures reach 0°C and melting occurs, the water may combine with alkaline dust, thereby neutralizing the acid components [Clausen et al. 2001]. Furthermore, the relation in Equation 3.2 assumes the ice to be completely frozen. As temperatures rise toward melting the relationship between the current and acid concentrations change, and above temperatures of -5°C surface conductance becomes possible through a water film, distorting the values [Clausen et al. 2001]. Temperatures during the measuring of the core often reached above -5°C , and peaks in the ECM values may therefore relate to currents measured in the water and not the ice. This problem is similar to that seen in the ice cores retrieved from the Hans Tausen ice cap [Clausen et al. 2001]. Despite the temperature problems related to the ECM data, large volcanic eruptions still produce distinct peaks at least 3 times the background variations, and these may be used as dating markers in the ice.

A plot of the ECM down through the ice core is shown in Figure 3.3. It is common to plot the values against the calculated acidity (from Equation 3.2) but due to the above mentioned temperature influence, the directly measured conductivity is given instead.

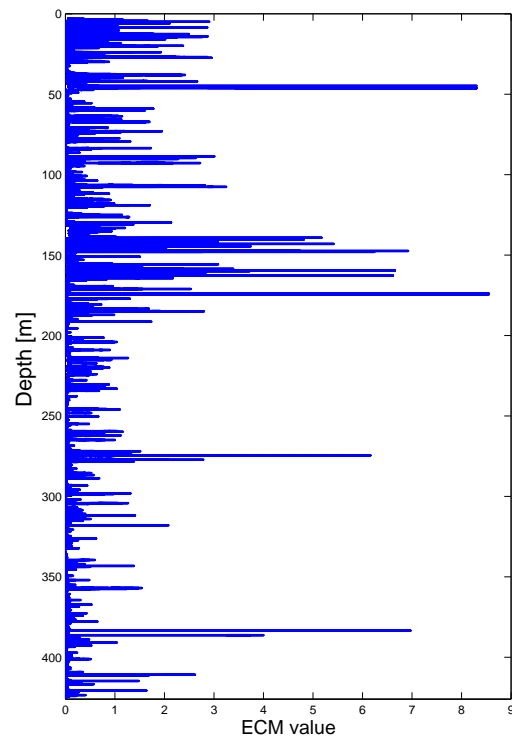


Figure 3.3: Plot of the parameter ECM down through the ice core. Note that the values are given in the directly measured conductivities and not the calculated acidity values, due to the temperature influence on the measurements.

3.3 Radar measurements

The application of radio-echo soundings in the study of ice caps was first used for determining the surface and bottom topography, and thereby the thickness of the ice. As methods have improved radio-echoes are now also used for exploring internal layers of the ice. It has become an invaluable method when investigating possible future drillsites, as basal melt rates, accumulation histories, ice flow and thickness may be estimated by the help of radio-echo data. The soundings may either be from airborne measurements or made directly on the ice. While it is more feasible to cover large areas in a short time with the airborne measurements, the downside is the loss of detail when compared with the direct measurements.

As mentioned in Chapter 3.2 the electrical conductivity changes down through the ice. As ice is a dielectric, the dielectric properties also change. This gives rise to the internal layers, since the power reflection coefficient R according to [Paren and Robin 1975], relates to the change in admittance of the ice by

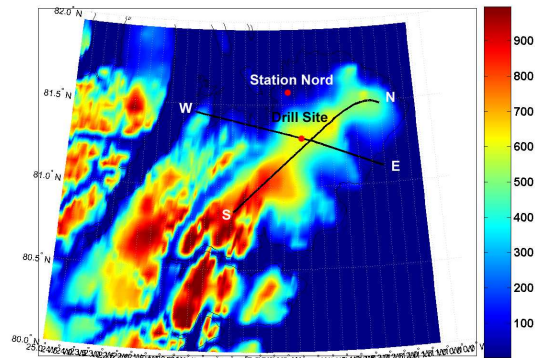
$$R = 4 \sin^2 \left(\frac{2\pi l}{\lambda_m} \right) \cdot \left| \frac{1}{2} \frac{\Delta Y}{Y} \right|^2 \quad (3.3)$$

where λ_m is the wavelength and l the thickness of the layer. Y is the admittance of the surrounding ice, while $Y + \Delta Y$ is the admittance in the layer. Changes in the admittance down through the ice is either due to impurities, temperature or compositional differences. This means that abrupt temperature variations,¹ volcanic activity and similar large-scale events usually create very distinct layers in the radar-echo soundings.

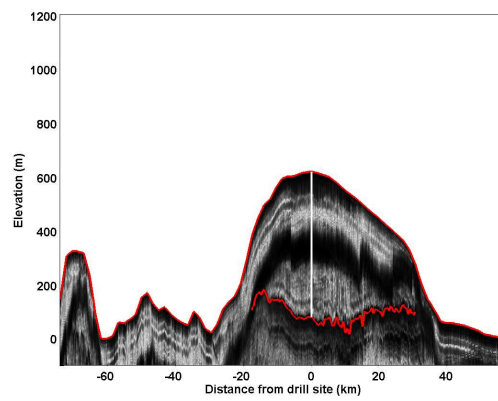
Airborne radio soundings were made above Flade Isblink in the summer of 1999 by Center for Remote Sensing of Ice Sheets (CReSIS), Kansas University. In Figure 4(a) is seen the flight lines of the measurements while Figures 4(b)–(c) show the actual measurements.

During the drill season in 2006, radar measurements were also undertaken directly on the surface with a radar mounted on a skidoo. Radar lines were measured on a grid around the drill site with a spacing of 1120 meters – roughly twice the ice thickness, H at the site. These measurements were to provide more detailed information of the internal layers in the ice cap. Melt layers in the ice will tend to weaken the radar signal, and the additional information from these measurements is very sparse as few internal layers are seen and none are distinguishable for a noticeable length. Therefore the main data from radar measurements, are from the overflights shown in Figure 3.4. These are used to estimate the ice thickness, bedrock height and topography and the extent of Flade Isblink ice cap.

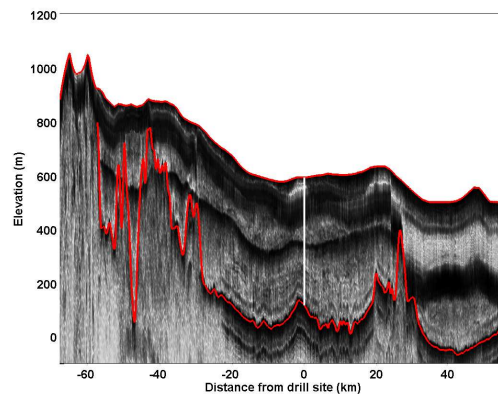
¹Such as the glacial → Holocene transition.



(a) Flight lines of the radar measurements performed in 1999. The values are height above sea level in meters.



(b) The radio-echo from the flight performed in the W-E direction.



(c) The radio-echo from the flight performed in the S-N direction.

Figure 3.4: Profiles of the Flade Isblink ice cap from radio-echo measurements made in 1999.

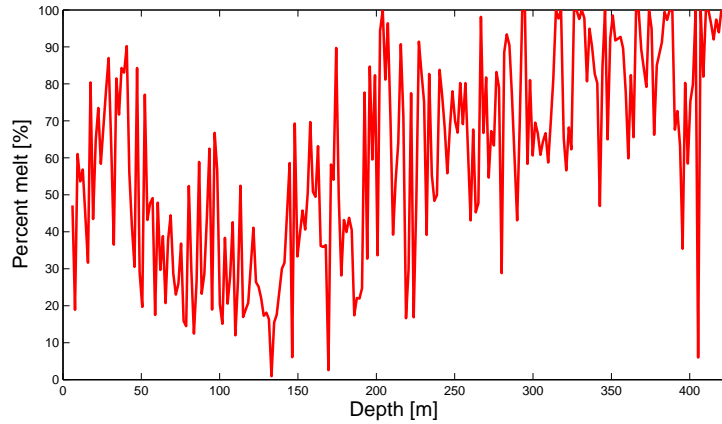


Figure 3.5: Plot of amount of melt in the ice down through the ice core.

3.4 Melt layers

Melt layers are present when the summer temperatures have been warm enough to melt the surface of the ice cap, causing meltwater to percolate through the underlying layers and refreezing further down [Koerner 1977, Koerner and Fisher 1990]. Melt layers are registered visually during the ECM measurements, as this refrozen ice is distinguishable from the ice created by compression in that it does not contain air bubbles.

As mentioned in Chapters 3.2 and 3.1 the melting of the ice cap produces problems when interpreting the $\delta^{18}\text{O}$ and ECM data. Likewise, the quality of radar measurements are reduced by melt layers. But every cloud has its silver lining, and the amount of melt in the ice may in itself give some evidence of the climatic variations that have taken place. The presence of a melt layer indicates that the equilibrium line was somewhere near the ice sheet surface at the time of deposition, and that temperatures must have reached above melting. In Figure 3.5 the amount of melt (in %) down through the ice core is shown.

3.5 Temperature measurements

The danish military has a permanent station, Station Nord which is located at $81^{\circ}36' \text{ N}$, $16^{\circ}40' \text{ W}$, some 20 km north of Flade Isblink. Originally built as a strategic station for the American air force in 1952, it now serves mainly as a permanent base for the Sirius patrol and for scientific expeditions during summer months. Daily temperature measurements have been carried out here since the early 1960s and in Figure 3.6 the average temperatures for the

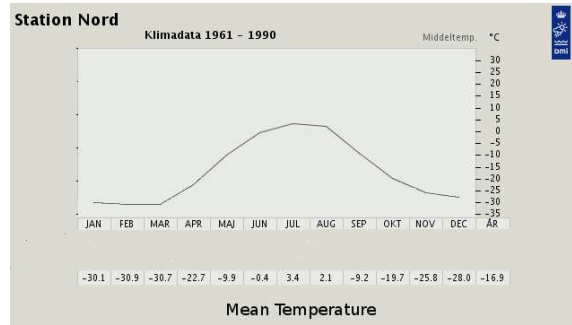


Figure 3.6: Average temperatures from 1961-1990 measured at Station Nord. Notice that even though the mean annual temperature is -16°C it often reaches above freezing during summer. Figure taken from <http://www.dmi.dk/>.

years 1961-1990 are shown. From the figure it is seen that average summer temperatures reach well above 0°C even though the average temperature is -16°C . As Station Nord is located some 500 meters lower in altitude than the drill site, the average temperatures on the ice cap will likely be some degrees lower. Still, temperature measurements from Station Nord may serve as a rough indication of what the present climate is like in the area around the ice cap.

3.6 Forcings

Where the previous chapter is concerned with the physical and temporal constraints that the model should reproduce, this chapter deals with the external forcings used to drive the ice flow model.

3.6.1 Mass Balance

The main forcing in the model is the mass balance on the ice cap. There are different ways to assess the accumulation rates back in time, which must be done since there is no direct information of previous values. One possibility of estimating past accumulation rates is by means of the $\delta^{18}\text{O}$ values. Analyzing the GRIP ice core, [Dahl-Jensen et al. 1993] found a strong correlation between $\delta^{18}\text{O}$ values and annual layer thicknesses. For this investigation that is not a feasible approach, since the $\delta^{18}\text{O}$ variations are too unreliable as a climatic proxy and likely cover too brief a period.

The present annual elevation change has been measured using data from the high-resolution satellite ICESat¹ [Pritchard et al. 2009]. This reveals a

¹Ice, Cloud and land Elevation Satellite.

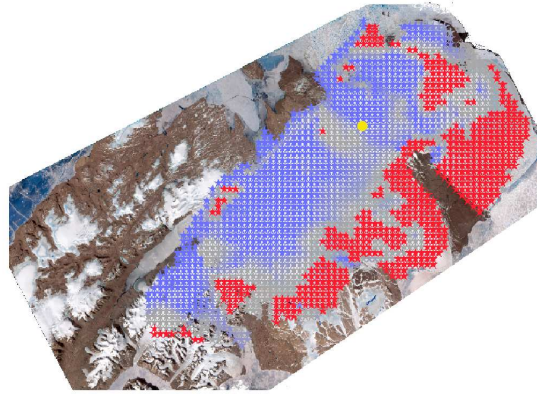


Figure 3.7: Elevation change of the Flade Isblink ice cap from measurements of the ICESat satellite spring 2004 - spring 2008. Blue indicates a positive elevation change, while red indicates negative. The drill site is shown with a yellow circle.

trend of growth (accumulation) in the western parts and loss (ablation) in the eastern parts of the ice cap. An ongoing investigation with a much higher resolution reaches the same general conclusions [Rinne pers. comm.]. Here is seen a growth of $\approx .5$ m/y in the western area, and a loss of $\approx .2$ -.3 m/y in the eastern parts. The current investigation also calculates the total annual volume gain of Flade Isblink, using both the Envisat Radar Altimeter 2 (RA-2) data and ICESat data. The RA-2 gives a volume gain of 0.89 ± 1.82 km³/y, while the ICESat shows a volume gain of 0.96 ± 1.72 km³/y (spring 2004 – spring 2008). Regardless of the exact values, these investigations establish that Flade Isblink is not in a steady state. In Figure 3.7 is seen a preliminary plot of the elevation changes measured from ICESat.

From the above values, a current mass balance rate at the drill site may be estimated. Furthermore the massbalance observations may be useful in bounding the current location of the equilibrium line when considering the location of the ablation zones. It should be noted that the applied mass balance curve will not be able to reproduce all features of the satellite data, as it is varied during the different model runs.

It should also be noted, that an explanation for the differences in annual elevation change is possibly found when considering the weather pattern at Flade Isblink, which may even explain why there is to be found an ice cap at all. Normally the cold winters at this latitude would result in relatively low accumulation rates due to lower amounts of vapour in the air. The large amounts of precipitation have been coupled with the fact that most of the sea east of the peninsula is ice free during winter months, and this water is likely

the main source of the snow ending on the ice cap. However, the prevailing surface winds in the area during wintertime are mainly northwestern and therefore not able to transport the air over the ice cap [Rasmussen 2004]. A weather pattern that may explain the situation is a pressure low over the arctic sea, that draws mild and humid air in from the east at high altitudes. Meanwhile cold, heavy winds near the surface blow from the northwest towards the low, and as they pass the ice cap, rise and force the precipitation from the high-lying warmer air. Most of the precipitation then lands on the western side of the ice cap, while the eastern (leeward) side is sheltered and gets less snow [Rasmussen 2004]. This would not only explain the distribution of precipitation, but also the ice free waters east of Kronprins Christians Land, as the strong winds push the sea ice away. Further evidence of strong northwestern winds comes from satellite images. During early summer, when the waters east of Flade Isblink are still ice covered, the images reveal large amounts of windblown dirt across the ice, for up to 50 kilometers out, originating from the snow-free parts of the peninsula west of the sea ice.

3.6.2 Temperature

As the modelled mass balance is dependent on $H^* - E$, the position of the equilibrium line must be estimated at each time step during the modelling. The temperature history at the surface of the ice cap is used to drive the height change of the equilibrium line with time. In this way the temperature together with the isostatic adjustment governs the height of the equilibrium line above bedrock, and thereby the annual mass balance.

First we must look at how the past temperatures may be estimated. As the $\delta^{18}\text{O}$ values in the ice core have been affected by melting, they cannot be used to reconstruct past temperatures at the surface of the ice cap. The temperature history used in this work is instead taken from reconstructions of past surface temperatures, using a Monte Carlo inverse method [Dahl-Jensen et al. 1998]. Precise measurements of borehole temperatures from GRIP were used to reconstruct the surface temperatures 50.000 years back in time. Similar measurements were performed at the DYE 3 drill site. In Figure 3.8 is seen the temperature anomalies at GRIP during the Holocene, with respect to 1995 values. Several distinct climatic events are distinguishable during the last 10.000 years: The Climatic Optimum covers the period 8-5000 years before present, where temperatures were ≈ 2.5 K warmer than present. The Medieval Warm is seen around 1 ky ago with temperatures ≈ 1 K warmer than present. Two cold periods are seen during the Little Ice Age around 400 years ago (at 1550 A.D. and 1850 A.D.). A slight warming is then seen until around 70 years ago (1930 A.D.) where-

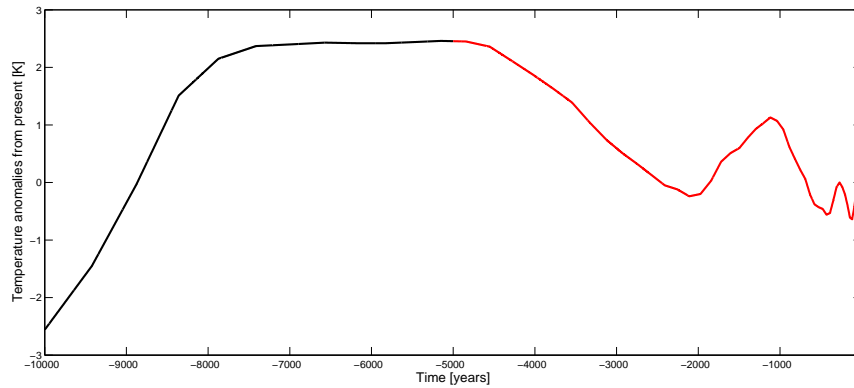


Figure 3.8: Temperature variations during the Holocene from inversions of GRIP bore hole measurements. The red part of the curve is the period used in this work. The notable climatic events that are seen are in good agreement with other climatic observations of the period. The Climatic Optimum is seen at 8-5 ky ago. The Medieval Warm around 1 ky ago, and two cold periods are seen during the Little Ice Age, 450 and 150 years ago. Temperatures reach a maximum around 70 years ago (1930 A.D.), with decreasing temperatures since then. Data taken from [Dahl-Jensen et al. 1998].

after temperatures decline steadily. These climatic variations are all seen in several other investigations [Dahl-Jensen et al. 1998].

The temperature reconstruction from the Dye 3 inversion shows the same variations during the last 7.000 years, but with amplitudes of the temperature anomalies about 50 % larger than at GRIP [Dahl-Jensen et al. 1998]. This indicates that the anomalies are regional but also that the exact amplitudes may not be the same at Flade Isblink, located approximately 1000 km north of GRIP.

The temperature history from GRIP is used as a forcing of the height of the equilibrium line. The temperature anomalies are taken with respect to year 1995 where measurements were made and set to zero subsequent years. As it is assumed the area was ice free during the Climatic Optimum, the period used in this work is the last 5.000 years, beginning just before the end of the Climatic Optimum. If the equilibrium line moves up and down with the atmospheric isotherm a change in temperature would amount to moving the equilibrium line by

$$\frac{dE}{dT} = -\frac{1}{\gamma}$$

Where $\gamma = -\frac{dT}{dz}$ is the atmospheric temperature lapse rate, often set as $\gamma = -6.5 \cdot 10^{-3}$ K/m. Using this value of γ would raise $E \approx 150$ m/K.

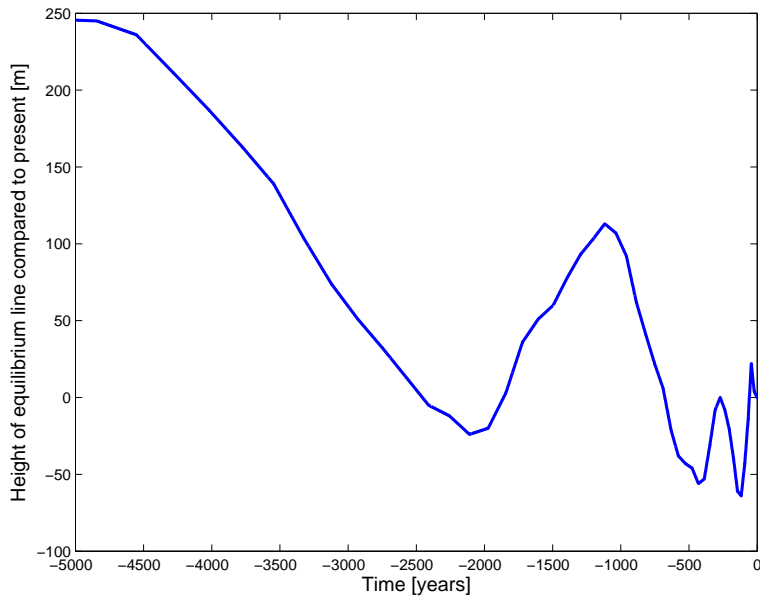


Figure 3.9: The temperature history taken from [Dahl-Jensen et al. 1998] leads to a forcing of the equilibrium line as shown.

Investigations have instead shown that a more appropriate value is to change $E \approx 100$ m/K [Oerlemans 2008], which is the value used in this work. This gives a forcing of the equilibrium line shown in Figure 3.9

In the modelling, the isostatic uplift and temperature history are kept fixed. Different models are achieved by varying the appearance of the mass balance curve, and the point at which the equilibrium line first crosses bedrock. The fact that the fixed parameters are not known with great accuracy does not affect the modelling much, as the mass balance curve is likewise not known better. A slight change in the equilibrium line height could for example be balanced by a different uplift history or mass balance curve, that would return the same modelled ice cap. Since the above mentioned parameters are all interrelated and none of them are precisely known, the choice of a fixed uplift and temperature change is therefore made.

4 Application of model

The ice flow model in combination with a dating model is used to simulate the buildup of the Flade Isblink ice cap. In this chapter the initial idealized setup is presented. The incorporation of the physical constraints in the model is explained, and various different modelled scenarios are tried. Of these, three models are presented and elaborated on. The present time where $t = 0$ is set as the time of drilling, 2006 A.D.

4.1 Initial setup

It is assumed that the ice core has been drilled on the summit. When looking at the radar profiles in Chapter 3.3 it is seen that the topography of the bedrock is very rugged – this is disregarded in the modelling. It is also assumed the ice cap is symmetric at the summit, which due to the differences in elevation change is also a simplification. The modelled profile is taken from the West-East going radar profile seen in Figure 4(b). The initial bedrock topography is simplified as shown in Figure 4.1. There is a slight rise¹ up to 180 meters, this is to have a starting point for the equilibrium line to cross and to better reproduce the current bedrock topography.

As bedrock was never reached during the ice core drilling, the exact ice thickness at the drill site is unknown. The best estimate is again from the radar soundings, that give values of the ice thickness, height and extent as follows

- $H^* = 620$ m
- $H = 540 \pm 10$ m
- $h = 80 \pm 10$ m
- $L \approx 25$ km

¹notice the different x and z scales.

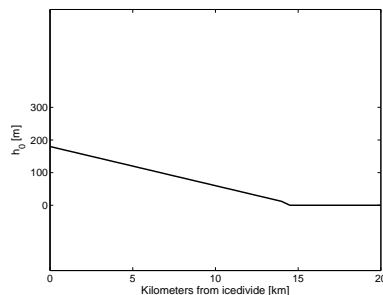


Figure 4.1: The initial bedrock topography in the model is simplified as shown in the figure. The slight inclination towards the ice divide is included to better reproduce the current bedrock topography.

Volcano	Year	Actual depth [m]	Ice equivalent depth [m]	λ [m]
Katmai	1912	44.8	40.8	.44
Laki	1783	89.4	82.4	.32
Unknown	1259	274.5	267.5	.35
Eldgjá	934	383.5	376.5	.34

Table 4.1: Data for the four volcanic events used as dating markers in the model.

The main constraint used in the modelling is the ice thickness, H , leaving the exact values of L , h and H^* more flexible.

From the ECM data there are 8 recognisable, dated volcanic events present in the ice core. The four most distinct events were used as a preliminary measure of the annual layer thickness, λ down through the core and as a constraint in the model. In table 4.1 the 4 eruptions are presented, with ice equivalent depth and the historic year in which they took place. The volcano Katmai is located in Alaska, while Laki and Eldgjá are found in Iceland. The origin of the 1259 eruption is unknown, but sulphate signals from this event are found both in Greenland and Antarctic ice cores, and the volcano is probably located somewhere near the Equator [Clausen et al. 1997]. Figure 4.2 shows the average annual layer thicknesses acquired from these four markers. From the volcanic markers it is seen that a simple mass balance history cannot fully explain the variations in λ , and that the ice cap is not in a steady state. The average layer thickness is almost constant down through half the ice cap and even rising with depth at one point.

It is assumed that the peninsula was ice covered during the last glacial, and that the ice melted away during the Climatic Optimum. This is similar to what is seen for other small ice caps in the Arctic [Koerner and Fisher 2002]. The models are then started when the equilibrium line crosses below bedrock, due to a combination of isostatic uplift that raises the bedrock and cooling

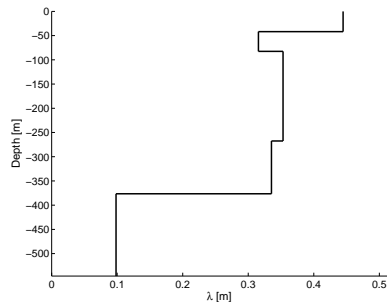
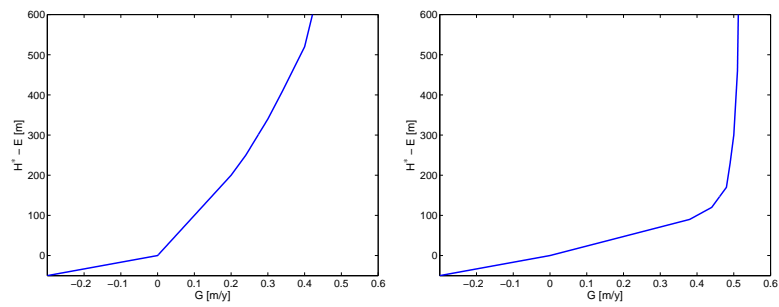


Figure 4.2: Annual layer thicknesses from the volcanic events registered in the ECM.

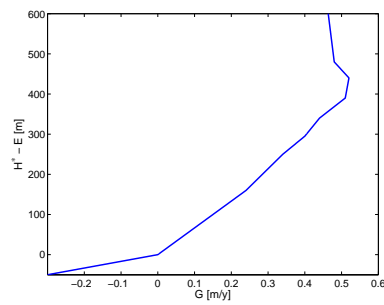
temperatures lowering the equilibrium line.

The first model starts at $t_{start} = -4000$ years and has a mass balance curve that is shown in Figure 3(a). The second run starts at $t_{start} = -2800$ years, with a mass balance curve as shown in Figure 3(b). The third and final model starts at $t_{start} = -3300$ years. The mass balance curve for this run is shown in Figure 3(c).

During the first run, the equilibrium line forcing is scaled down to 80%. This is purely for modelling reasons so the equilibrium line will not descend far below the entire bedrock area. This downscaling may be almost completely balanced by the appearance of the mass balance curve. The other two runs have the same forcing as shown in Figure 3.9.



(a) Mass balance curve for the first scenario. (b) Mass balance curve for the second scenario.

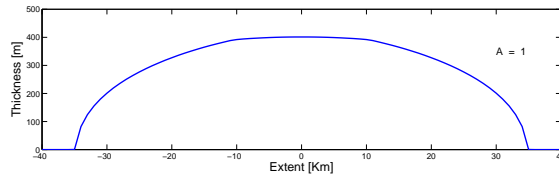


(c) Mass balance curve for the third scenario.

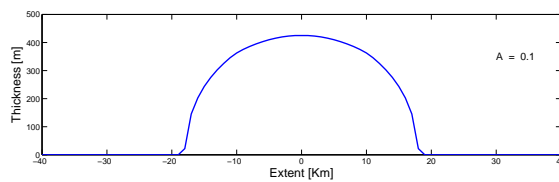
Figure 4.3: Mass balance curves for the three different model runs.

5 Results

Some preliminary runs were performed with a simple setup, in order to investigate the influence of the various parameters. Two runs were made with the value of A from Equation 2.12 set as $A = 1$ and $A = 0.1$, respectively. Both scenarios were run for 6.000 years on a flat bed, with no isostatic adjustment and a constant accumulation when $H^* > 0$. The results are seen in Figure 5.1.



(a) Value of parameter $A = 1$



(b) Value of parameter $A = 0.1$

Figure 5.1: Two profiles of the ice cap after 6000 years, showing the influence of A on the shape of the ice cap. In (a) the value is set to 1, and in (b) the value is 0.1. In (b) the ice cap is about 5 percent thicker at the divide but extending considerably less horizontally. Note that neither ice cap is in steady state, both are still growing.

Note that the total volume in Figure 1(a) is larger than in 1(b) due to the larger area where accumulation is possible.

The value used by [Oerlemans 1981] is $A = 1$. This value is used when modelling the Greenland Ice Sheet with a height to width ratio of $\approx 10^{-3}$.

A scale analysis of the Flade Isblink ice cap yields a height to width ratio of $\approx 500 \text{ m}/50 \text{ km} = 10^{-2}$. It therefore seems reasonable to apply a value of A an order of magnitude lower than that used to model the Greenland Ice Sheet.

5.1 Age of the ice cap

The evolution at the ice divide during the first model run is seen in Figure 5.2. Here is shown the height, thickness and mass balance changes at the divide. The fourth subfigure depicting $G - \frac{dH}{dt}$ is included to better understand the thinning induced by the flow. The value of $G - \frac{dH}{dt}$ relates to the ice flow as seen in Equations 2.24 and 2.25. During the initial buildup of the ice cap the value is close to zero. This indicates that almost no thinning takes place, which is as expected. As the ice cap grows, the value rises and the ice flow becomes more dominant in determining the total height change.

In Figure 5.3 is seen the size of the ice cap at different times during the buildup. The height of the equilibrium line is shown in red, while bedrock $h(x)$ is shown in black. The first figure shows the scenario just as E crosses bedrock at $t = -4000$ years. During the buildup the cap is steadily growing, slowly at first due to the lower accumulation rate, but after about 1000 years a relatively steady growth is seen. The present modelled ice cap is shown in the final figure, where $t = 0$ years.

After the buildup has been modelled, the age down through the ice cap is estimated. A depth-age plot of the modelled ice cap is seen in Figure 5.4. Also depicted with red stars are the ice equivalent depths where the four volcanic markers are found in the ice core data.

The final results presented from the first model run are shown in Figure 5.5. In (a) The mass balance at the divide is shown in green, while the height of the surface above E is shown in blue. In (b) the annual layer depth down through the ice is shown in blue, while the original mass balance is shown in red¹. The difference between the red and blue curve relates to thinning of the layers due to compression and flow. The black curve shows the mean λ values from the four volcanic markers. In order for the model to reproduce the volcanic marker depths, the mean values of the blue curve should equal those of the black curve, for a given depth interval.

Similar figures to the ones shown above are also presented for the second model run, starting at $t = -2800$ years. The figures relating to the second run are Figures 5.6 – 5.9. The features seen around $t = -2500$ years in the three lowest figures in Figure 5.6 are a result of the appearance of the

¹The red curve in (b) is the same as the green curve in (a).

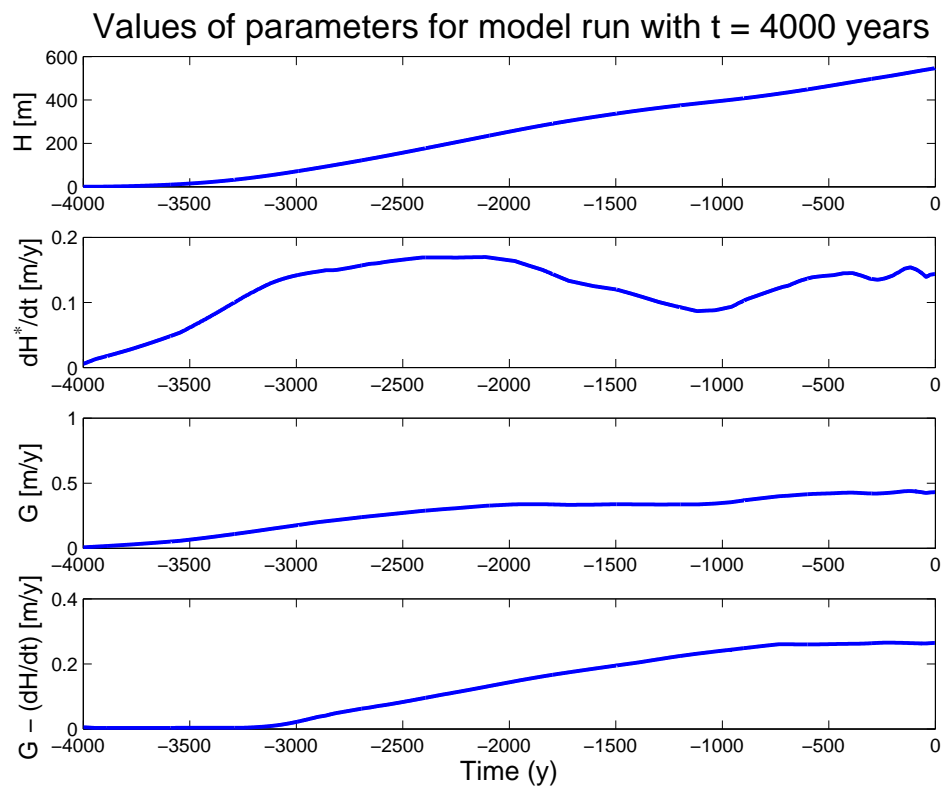


Figure 5.2: Four values relating to the ice divide appearance during the first model run. The upper figure shows the ice thickness at the divide, while the second shows the change of surface height with time. The third depicts the mass balance, while the fourth shows the value $G - \frac{dH}{dt}$, crucial to the flow of the ice.

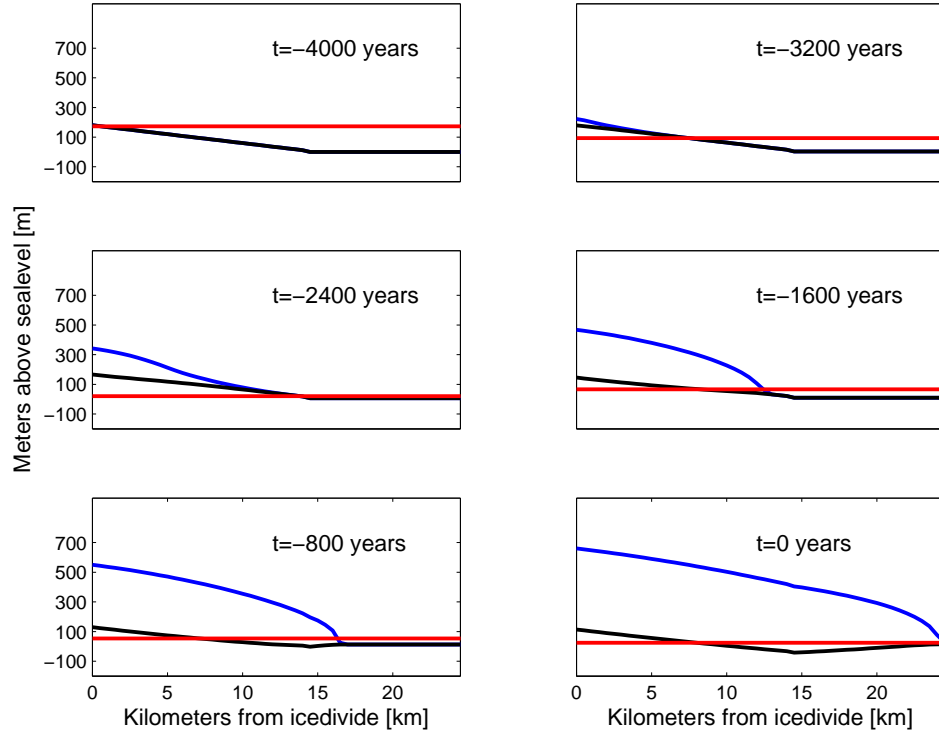


Figure 5.3: 6 snapshots of the buildup of the ice cap at different stages during the first model run. The blue curve is the height of the ice cap surface. The height of the equilibrium line is shown in red, while the bedrock is shown in black.

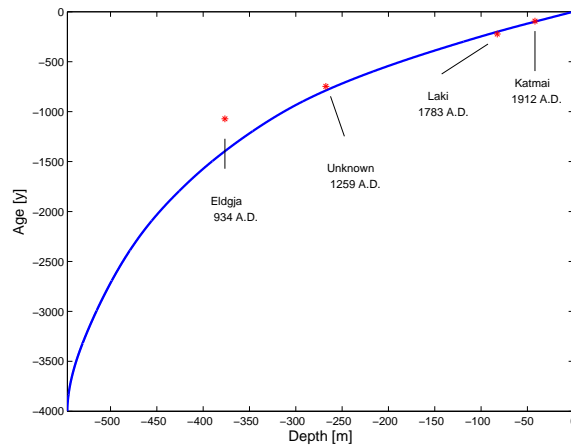
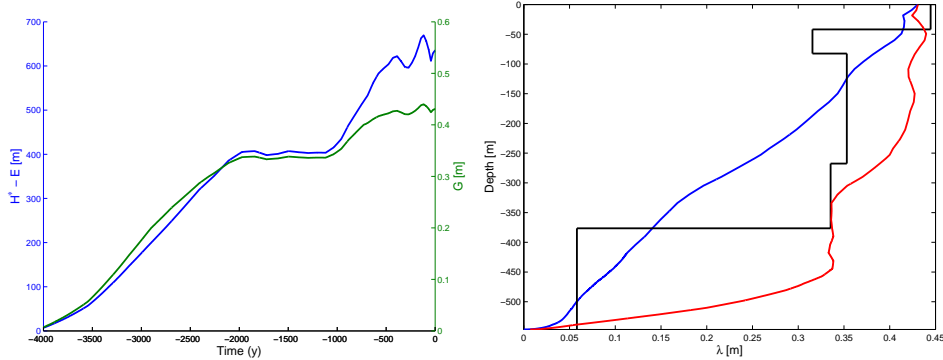


Figure 5.4: Depth-age plot at the ice divide for the first model run. The four red stars indicate the ice equivalent depths at which the volcanic markers are found in the ice core.



(a) The blue curve shows the surface height above E , while the green curve shows the annual layer thicknesses, while the red line gives the mass balance at time of deposition. The black curve shows the average λ values between the volcanic markers – it is identical to the curve in Figure 4.2

Figure 5.5: Two plots of the mass balance and annual layer thicknesses back in time for the first model run.

mass balance curve applied. Around a value of $100 < (H^* - E) < 200$ meters, the rate of mass balance increase with height drops rapidly, leading to the change in the parameters shown in the figure. The data relating to the third model run is shown in Figures 5.10 – 5.13. The peak seen in the mass balance around $t = -1000$ years in Figure 5.13 is due to the height dependence of the mass balance around $(H^* - E) \approx 400$ meters.

A comparison of the 3 different depth-age scales acquired is shown in Figure 5.14. Here the green curve shows the values for the first model run, the blue curve shows the second run and the black curve shows the values from the third run.

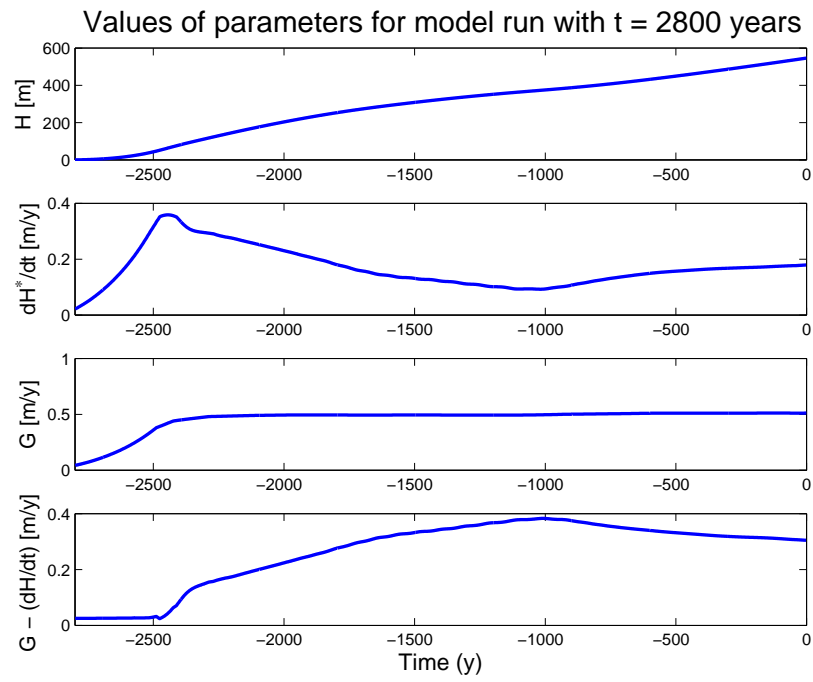


Figure 5.6: Four values relating to the ice divide appearance during the second model run. The upper figure shows the ice thickness at the divide, while the second shows the change of surface height with time. The third depicts the mass balance, while the fourth shows the value $G - \frac{dH}{dt}$, crucial to the flow of the ice.

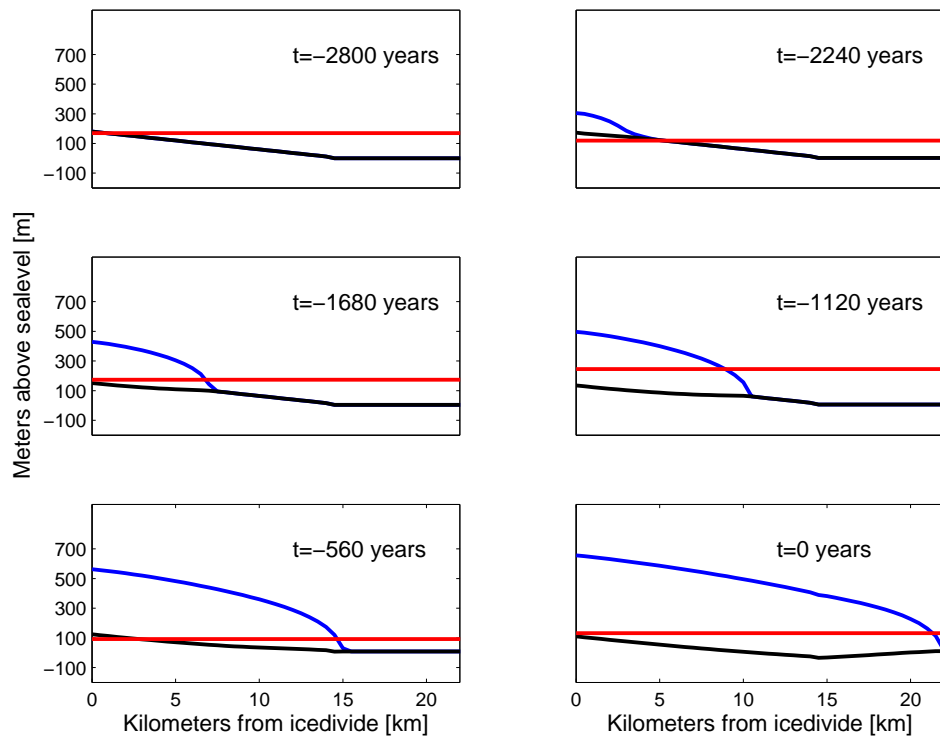


Figure 5.7: 6 snapshots of the buildup of the ice cap at different stages during the second model run. The blue curve is the height of the ice cap surface. The height of the equilibrium line is shown in red, while the bedrock is shown in black.

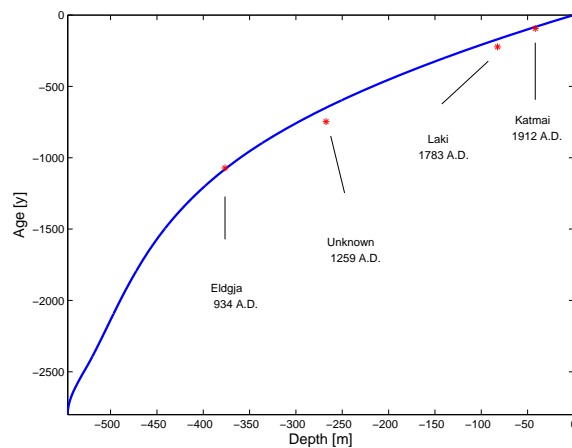
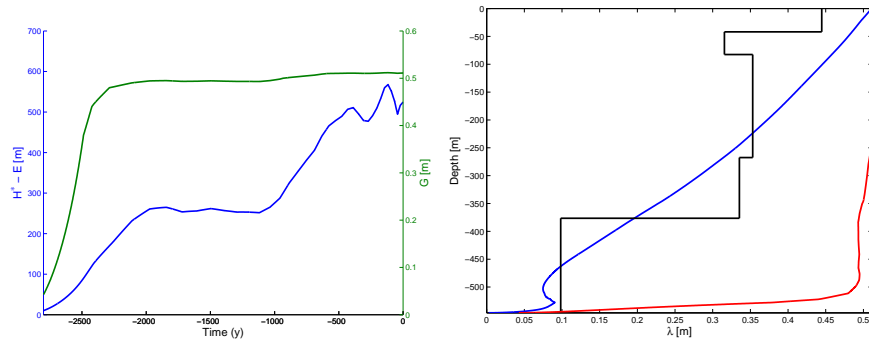


Figure 5.8: Depth-age plot at the ice divide for the second model run. The four red stars indicate the ice equivalent depths at which the volcanic markers are found in the ice core.



(a) The blue curve shows the surface height above E , while the green curve shows the annual layer thicknesses, while the red curve shows the mass balance at the ice divide. (b) The blue line indicates the modelled annual layer thicknesses, while the red line gives the mass balance at time of deposition. The black curve shows the average λ values between the volcanic markers.

Figure 5.9: Two plots of the mass balance and annual layer thicknesses back in time for the second model run.

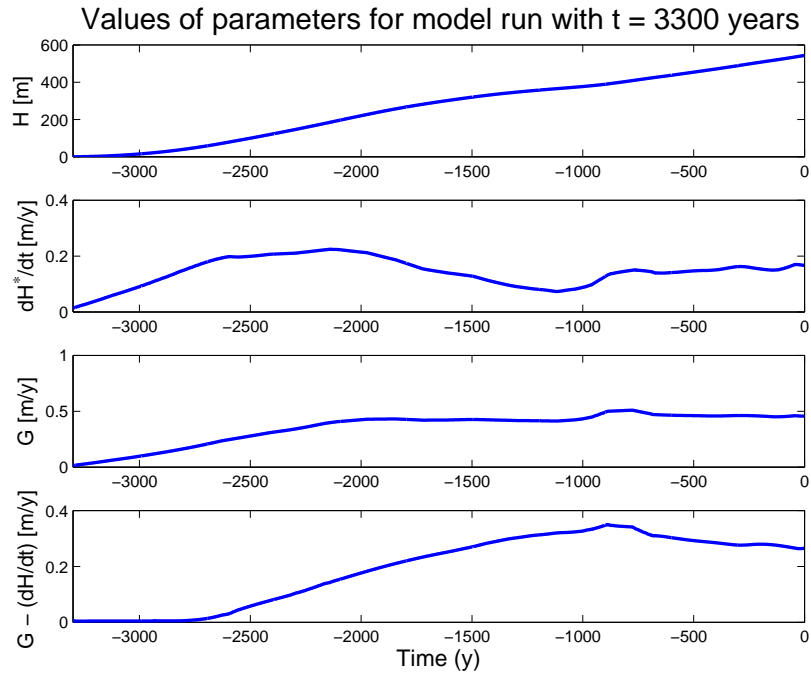


Figure 5.10: Four values relating to the ice divide appearance during the third model run. The upper figure shows the ice thickness at the divide, while the second shows the change of surface height with time. The third depicts the mass balance, while the fourth shows the value $G - \frac{dH}{dt}$, crucial to the flow of the ice.

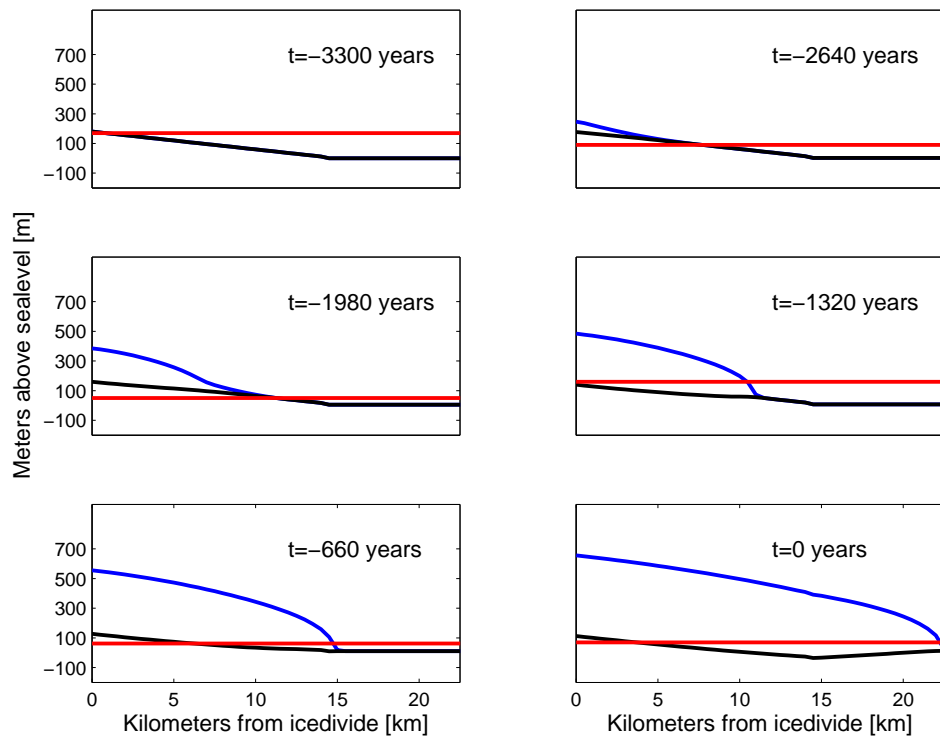


Figure 5.11: 6 snapshots of the buildup of the ice cap at different stages during the third model run. The blue curve is the height of the ice cap surface. The height of the equilibrium line is shown in red, while the bedrock is shown in black.

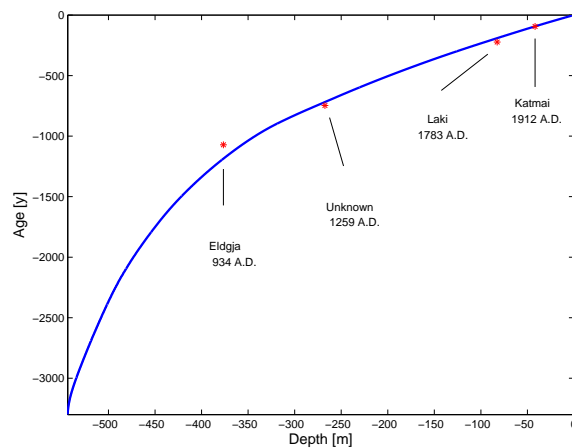
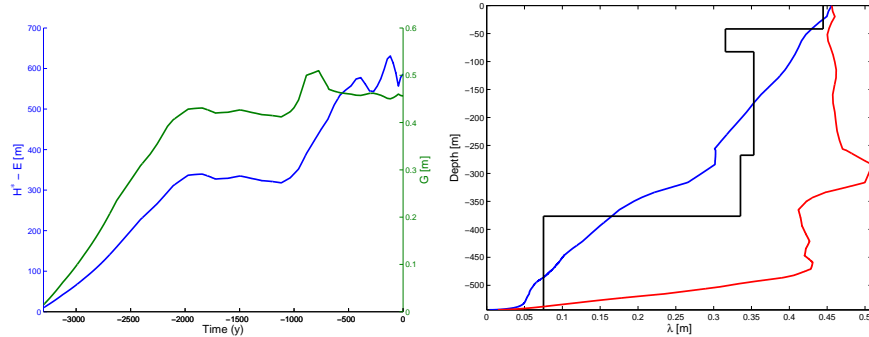


Figure 5.12: Depth-age plot at the ice divide for the third model run. The four red stars indicate the ice equivalent depths at which the volcanic markers are found in the ice core.



(a) The blue curve shows the surface height above E , while the green curve shows the mass balance at the ice divide. (b) The blue line indicates the modelled annual layer thicknesses, while the red line gives the mass balance at time of deposition. The black curve shows the average λ values between the volcanic markers

Figure 5.13: Two plots of the mass balance and annual layer thicknesses back in time for the third model run.

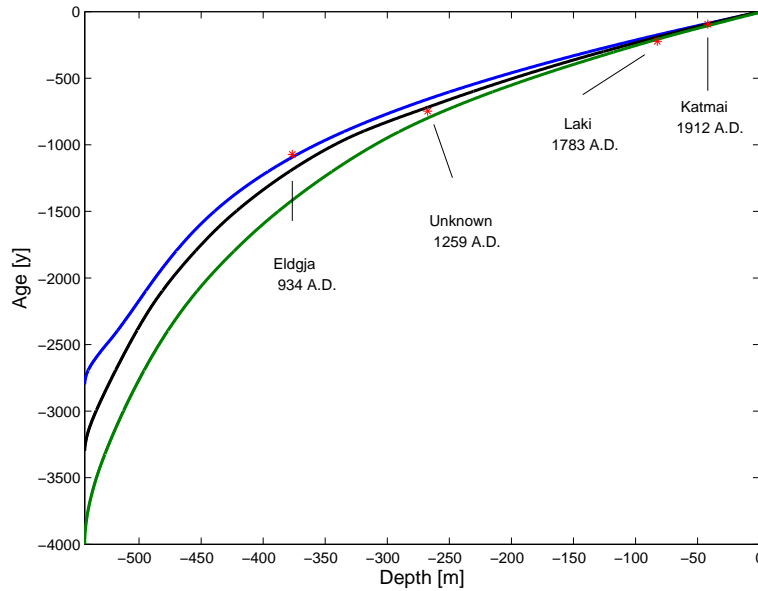


Figure 5.14: The depth-age relationship for the 3 different model runs are plotted together. The blue curve is from the second run, while the black and green are from the third and first run, respectively.

6 Discussion

The strengths and weaknesses of the three different buildup histories are analyzed in this chapter. A time scale is chosen for investigating climatic variations, and the results are discussed. The total knowledge from the Flade Isblink ice cap is scarce, and the model variables and degrees of freedom are many. This must be borne in mind when regarding these simple models.

All three models produce the current position of the equilibrium line somewhere near the bottom of the ice cap. From the satellite observations, it is more likely that the actual position is a bit higher, due to the relatively large ablation zone on Flade Isblink. The modelled current position is mainly due to the fact that the temperature forcing lowers $E \approx 100\text{--}200$ meters during the different model runs, and as the model starts when the equilibrium line first crosses bedrock (180 meters above sealevel) this leaves the current position near the bottom. The exact current position of E is maybe not so important though, seeing as the accumulation history is not better known. There is also still a small ablation zone in all models.

None of the three modelled runs are able to re-create all the average annual layer thicknesses between the four volcanic markers. In Figure 6.1 the amount of annual layer thinning for the second model run is shown, calculated by the formula

$$\left(1 - \frac{\lambda}{\lambda_0}\right) \cdot 100\%$$

where λ_0 is the original layer thickness, and λ the present thickness. The amount of thinning rises towards the bottom, as the lower layers have experienced the thinning effects for a longer time than the layers above. This increased thinning of annual layers implies that a simple mass balance curve, steadily growing with $(H^* - E)$ will not be able to reproduce all 4 volcanic

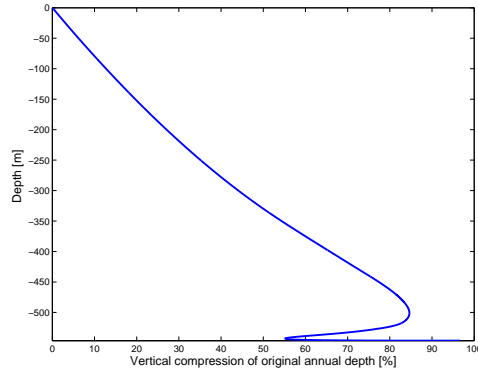


Figure 6.1: fraction of the original layer thickness at a given depth. The thinning of the layers with time leads to the curve shown.

depths. The first model starting at $t = -4000$ years, is able to re-create the depths of the three youngest volcanic markers accurately, while the remains of the Eldgjá eruption is found several tens of meters lower than what the model predicts. The second model run re-creates the depths of the youngest and oldest volcanic markers almost exactly, but at the expense of the traces from Laki and the 1259 A.D. volcano being modelled too far down in the ice. The third run represents the best possible fitting of the four volcanic depths, using the simple flow model. It models the Laki and 1259 A.D. volcanic markers only a little below their actual depths, while greatly lowering the Eldgjá depth discrepancy found in the first model.

Even though no model captures all details seen in the volcanic markers, the three scenarios may still be able to bound the age of the Flade Isblink ice cap to some extent. This will be regarded in the following section.

Upper age limit:

In the first model that produces the oldest age for the ice cap, the trace of Eldgjá is modelled nearer the surface than the actual depth where it is found. This means that the average layer thickness above this depth is thinner in the model than what is actually the case. As the value of $h_k = 0.2H$ the uppermost layers already experience relatively little thinning, and lower values of h_k are probably not realistic. As the three youngest volcanic markers are found reasonably close to their modelled depths, this means the discrepancy in annual thicknesses must be found below the depth of the 1259 A.D. volcano. If the ice cap is older than the first model calculates this would then make the discrepancy of the Eldgjá depth even larger, as buildup must have started during warmer times and the average annual depths in the lowest layers must be even thinner. An upper age limit of the ice cap is therefore set to 4000 years.

Lower age limit:

Using the temperature forcing from the GRIP curve entails a lower boundary for the youngest possible ice cap age. By regarding Figure 3.9, an ice cap starting to build up after $t = -2800$ years, would most likely melt away during the Medieval Warm. It is not plausible that the climate would only become cold enough to support the buildup of an ice cap after $t = -2800$ years, since this would leave too brief a period to accumulate an ice cap able to survive the subsequent raising of the equilibrium line. Either this or an unrealistically high mass balance ($G > 1$ m/year) is needed to be reached just after the buildup has started. This in turn would place the modelled youngest volcanic markers significantly below their actual depth. Due to the presence of the Eldgjá marker, the ice cap can most definitely not have built up after $t = -1100$ years. These considerations put a lower age limit on the ice cap at 2800 years.

Comments on mass balance curve: While the first two models apply a mass balance steadily growing with height, the mass balance curve applied in the third run does not. Instead it reaches a maximum around $H^* - E = 400$ meters, whereafter it declines with height. The low altitude of the ice cap surface makes it unlikely that a maximum mass balance should have been reached, as H_{max} is most likely found well above 1000 meters above sea level [Dahl-Jensen, pers. comm.] This model run is included to get the best possible fit with all 4 volcanic depth markers. Even with this shape of the mass balance, the model is not able to reproduce the depths exactly. This of course is also a reflection on the fact that the model applied is simplified and many parameters may influence the modelled age down through the ice. Here it should also be noted that the ice cap may have changed accumulation source over the buildup period. As the ice cap grows, the increase in surface height raises the lowest possible height for clouds to form precipitation over the ice. The nature of the windpattern and local source of precipitation mentioned in Chapter 3.6.1 is very likely to play a role in the evolution of the ice cap.

From the modelled results, we bound the age of the ice cap between 2800 and 4000 years. When regarding the model age of the ice cap, reproducing the depth of the oldest volcanic marker implies that the average modelled layer thickness down to this fixpoint is correct. The youngest and oldest volcanic markers are satisfactory fixpoints in the second model, and from Figure 5.14 it is seen that the discrepancy of the Eldgjá depth marker rises with the model ages. Therefore it seems likely that the models setting the younger ages are closer in reproducing the correct ice cap age. The best estimate of the Flade Isblink ice cap age is therefore set between 2800 and 3300 years.

6.1 Applying the time scale to climatic proxies

From the above considerations we assume an age of the ice cap somewhere between 2800 and 3300 years. As the mass balance for the third run is assumed unrealistic, the time scale from the second model run is applied to the recorded melt layers and $\delta^{18}\text{O}$ values. As mentioned in Chapter 3.4 the presence of melt layers indicate that summer temperatures were warm enough to melt the upper layers. A change in the percentage may indicate a change in summer temperatures, but it may also indicate a change in accumulation rates – if for example the accumulation rate drops, but temperatures stay the same, the relative amount of snow that is melted would be larger.

A study of melt layers was performed on three ice cores retrieved from the Devon Island ice cap located in the Canadian Arctic [Koerner 1977]. This study reveals that melt layers in the ice core reflect not only local but regional climatic variations. It also concludes that meltwater may percolate down through several years of snow layers whereby the resolution in a melt layer may cover several years.

In Figure 6.2 The amount of melt layers found in the ice core is shown in red. The blue curve shows the modelled surface height above E . The melt values in the upper part are misrepresented a bit as the surrounding firn densities are below that of the ice. But as average densities are never much lower than that of solid ice, this error is small, and the directly measured melt layer percentages are used for simplicity. Putting the melt layers on a time scale may provide some insight in the climatic history during the most recent Holocene, as large amounts of melt is a good indication of warm summer temperatures. The surface height above E is naturally affected by elevation changes of the ice cap surface and in a study of the Canadian high-Arctic Agassiz ice cap, approximately 40% of the amount of melt layer change was contributed to changes in the surface height [Koerner and Fisher 1990].

The $\delta^{18}\text{O}$ values are also put on a time scale. In Figure 6.3 the $\delta^{18}\text{O}$ values are seen in blue, while the melt percentage is seen in red. Just like the meltlayers, a part of the variation in the $\delta^{18}\text{O}$ signal is due to elevation change of the ice cap surface, which does not reflect a regional climatic change. This variation may be evaluated by the following consideration. Assuming the current relation of $1.5^\circ\text{C}/\text{‰}$ mentioned in Chapter 3.1 and the lapse rate from Chapter 3.6.2, an elevation change of 540 meters would infer a lowering of the oldest $\delta^{18}\text{O}$ values by $\approx 3 \text{ ‰}$.

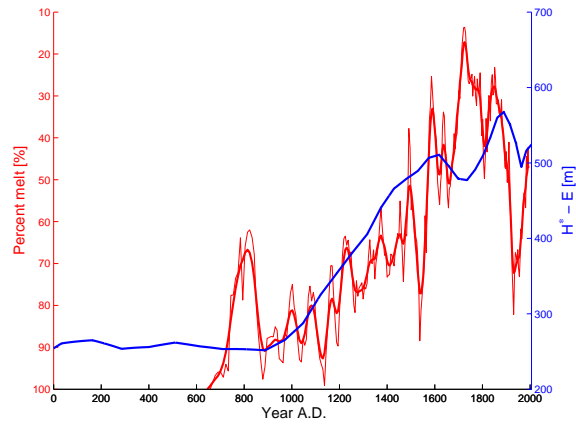


Figure 6.2: The amount of melt plotted on a time scale along with the surface height above the equilibrium line. Notice the inverted Y-axis for the melt percentage.

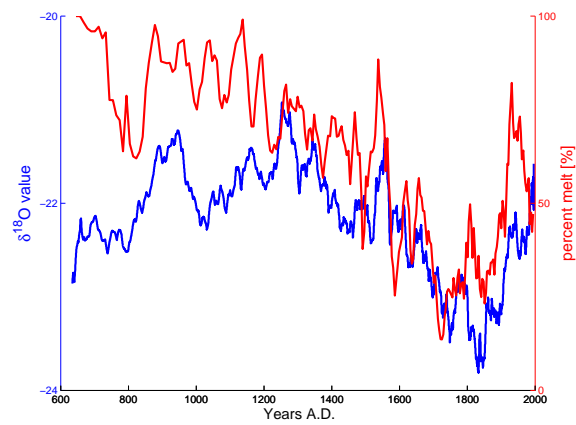


Figure 6.3: The $\delta^{18}\text{O}$ values (blue) plotted on a time scale from model run 2, along with the percentage of melt layers (red).

6.2 Discussion of climatic proxies

The melt layers show evidence of well known climatic changes during the most recent Holocene. As the time scale applied is not definitive, a detailed study of the climatic events is not made. Indications of the Little Ice Age is seen in low values of the melt percentage between 1500-1800 A.D. while a sharp rise in melt percentage is seen around 1920 A.D. When comparing the melt percentage curve to the height above E in figure 6.2, the two curves seem to be in general agreement, albeit with notable differences. In the melt layers there is a sharp decline in the amount of melt around 800 A.D. (just before a possible Medieval Warm) that lasts for about 100 years. This would indicate a cooling or perhaps a change of accumulation rates, while during the same period, the surface height above E is almost constant. Another noticeable feature is that the amount of melt seen during the 1920-1930 warm is not proportional to the change in $(H^* - E)$ but shows a larger change, indicating that this may have been a larger climatic event in north eastern Greenland, than at GRIP. At this point it should be noted that the modelled location of the equilibrium line at this time is probably lower than the actual height, maybe indicating that the drop in $(H^* - E)$ at this period should be larger. The general agreement between the melt layer data and the modelled surface heights strengthens the assumption of a young ice cap.

Some climatic variations present in the melt layers are also seen in the $\delta^{18}\text{O}$ signal. The $\delta^{18}\text{O}$ curve correlates with the variations in melt for a large period, back until around 1200 A.D. Going further back, the $\delta^{18}\text{O}$ value steadily decreases, even though melt layers indicate a rise in temperature back in time. This apparent conflict may be explained by noting that during the warmest times, when melt percentages are high, the snow accumulating during summer melts away, leaving the winter snow to dominate the $\delta^{18}\text{O}$ values. As the cold winter $\delta^{18}\text{O}$ values may be 7-8 ‰ lower than summer values [Dahl-Jensen, pers. comm.] this would easily explain the difference. A less readily explained difference is seen during the last century. The amount of melt percentage has dropped steadily since around 1930 A.D. while the $\delta^{18}\text{O}$ values continue to rise.

The general trend of rising amount of melt towards older times may be seen as a consequence of the ice cap starting to grow, when the equilibrium line crossed bedrock. This means the surface height must have been just above the equilibrium line for a long period in the beginning of the buildup. We do not have melt layer records for the bottom 115 meters of the ice cap, but it would seem likely that values would be at or near 100% melt. This may be highly influential on the mass balance scenario, as some of the meltwater may not refreeze, but form run-off. This is consistent with previous studies indicating a high correlation between melt layer ice percentage and the mass

balance of the ice cap [Koerner 1977]. This implies that especially the oldest layers in the ice may be thinner than the model simulates, indicating an older ice cap than assumed here.

6.3 Future of the ice cap

Assuming an age of the Flade Isblink ice cap of approximately 3000 years, some considerations on future scenarios can be made. Temperatures from the GRIP core reveal that the temperatures during the Climatic Optimum were only a few degrees warmer than around 3000 years ago. If the ice covering Kronprins Christians Land melted away when temperatures were just a couple of degrees warmer, this would also be a likely scenario for the present ice cap if temperatures rise as indicated by the projected preferential warming in the arctic region [Anisimov et al. 2007]. Especially considering that climate change in the arctic is amplified by several feedback factors [Overpeck et al. 1997]. There are also indications from satellite observations that the two outlet glaciers located north east of the ice cap have surged recently [Rinne pers. comm.], and melting of glaciers and ice caps such as Flade Isblink is likely to contribute significantly to future rises in sea level [Meier et al. 2007].

7 Conclusion

A modelling has been made of the buildup of the Flade Isblink ice cap, using a vertically integrated 1D model with a height dependent mass balance. The main constraint on the model is from ice core data, providing four known volcanic markers down through the ice core. Three different scenarios are presented that all to some degree reproduce the constraints on the ice cap, but none conclusively. The age of the ice cap is bounded between 2800 and 4000 years due to the modelled results – most likely nearer the younger age. No definitive age can be determined from the simple model applied, as the constraints from volcanic reference markers are not consistent with a simple mass balance growing with altitude.

A time scale is set up based on an age of 2800 years. The melt layers seen in the ice are put on a time scale and compared to other records of climate change. Evidence of several well known climatic events is seen in the melt layer data, and comparing these to the modelled surface heights above the equilibrium line strengthens the assumption of a young ice cap.

7.1 Outlook

A 2D model would probably not be able to reveal much more information on the ice cap, since the data from Flade Isblink is so scarce. In order to attain a more precise buildup history of Flade Isblink, more information must be gathered. A more detailed look at the melt percentages and implications for mass balance changes perhaps would be more fruitful. The time scale provided from this work, may be used as a first approximation for the melt percentages at a given time, and this may be used to affect the mass balance accordingly. It is possible that this may provide an explanation for the otherwise puzzling variation of annual layer thicknesses down through the core. Another possibility is to apply a more dynamical model, allowing for

surges of outlet glaciers, as the one proposed to have happened recently. This may also help in producing a buildup history that better fits the constraints.

With a better understanding of the climate sensitivity of the ice cap, it would also be interesting to model future scenarios for Flade Isblink. It seems likely that a few degrees warming would be able to melt the ice cap away just as happened during the Climatic Optimum.

A Matlab code

A.1 Main program

```
1  %% Programme to model the evolution of Flade Isblink 2006
2  %M-filer der kaldes i dette program...
3  %constants, E_profile, Date (Tracedown), Figurer
4
5  constants          %call constants and
6  E_profile          %Generate the temporal evolution of the equilibrium line
7
8  %%%%%%%%%%%%%%% initial profile
9  h_0=zeros(N,1);
10 h_0(1:29)=(180:-6:12);
11 h=h_0;
12 E_start=h(1)*ones(N,1)-;
13
14 for i = 1:M
15
16  % % % % % clear old values of matrices/vectors
17  dD_dx=          zeros(N,1);
18  D=              zeros(N,1);
19  alpha=          zeros(N,1);
20  beta=           zeros(N,1);
21  A_matrice=      zeros(N,N);
22  B_matrice=      zeros(N,N);
23  C_vektor=       zeros(N,1);
24  G=              zeros(N,1);
25  H_star=         zeros(N,1);
26  E=              zeros(N,1);
27
28  H_star=H+h;
29  E=E_start+E_temp(end-M+i)-E_temp(end-M);
30  H_over=H_star-E;
31  G_calc          %Calls programme to calculate G
32  C_vektor=G*dt;
33
34  h=h-(1/(2*T_iso))*(H+6*(h-h_0))+40/10000*dt; %isostatic adjustment
35  h_0 = h_0+40/10000*dt; %change of h, due to previous load
36
37  %%%%%%%%%%%%%%% find components of A and B matrices %%%%%%%%%%%%%%%
38
39  % % % D(j+1)=D(j) -- gives beta
40  D(1)=D_0;
41  D(2:N-1)=A*H(2:N-1).^(m+1).*((H_star(3:N)-H_star(1:N-2))/(2*dx)).^2).^(m-1)/2);
42  D(N)=A*H(N)^(m+1)*abs(((H_star(N)-H_star(N-1))/(dx)))^(m-1);
43  D(2)=interp1([x(1),x(3:N)'],[D(1),D(3:N)'],x(2),'pchip');
44  D(N-1)=interp1([x(1:N-2)'],x(N),[D(1:N-2)'],D(N),x(N-1),'pchip');
45  D_under=find(D<D_0);
46  D(D_under)=D_0;
47  beta=D*dt/(2*dx^2);
```

```

48 % % %
49
50 % % % dD_dx(j+1)=dD_dx(j) -- gives alpha
51 dD_dx(1)=(D(2)-D(1))/dx;
52 dD_dx(2:N-1)=(D(3:N)-D(1:N-2))/(2*dx);
53 dD_dx(N)=2*dD_dx(N-1)-dD_dx(N-2);
54 alpha(2:N)=dD_dx(2:N)*dt/(4*dx);
55 % % %
56 for i=2:N-1
57     A_matrice(i,i-1)=alpha(i)-beta(i);
58     A_matrice(i,i)=1+2*beta(i);
59     A_matrice(i,i+1)=-alpha(i)-beta(i);
60     B_matrice(i,i-1)=beta(i)-alpha(i);
61     B_matrice(i,i)=1-2*beta(i);
62     B_matrice(i,i+1)=alpha(i)+beta(i);
63 end
64
65 %%%%%%%%%%%%%%%%%%%%%%%%%%%%%%%%%%%%%%%%% boundary conditions
66 k=dt*(D(2)-D(1))/(4*dx^2);
67 %
68 A_matrice(1,1)= 1+5*k;
69 A_matrice(1,2)= 1-4*k;
70 A_matrice(1,3)= -k;
71 A_matrice(N,N-1)= 2*alpha(N); %alpha(N)-beta(N);
72 A_matrice(N,N)= 1-2*alpha(N); %1-alpha(N)+beta(N);
73 %
74 B_matrice(1,1)= 1-5*k;
75 B_matrice(1,2)= 1+4*k;
76 B_matrice(1,3)= k;
77 B_matrice(N,N-1)= -2*alpha(N); %-3*alpha(N)-beta(N);
78 B_matrice(N,N)= 1+2*alpha(N); %1+3*alpha(N)+beta(N);
79 %%%%%%%%%%%%%%%%%%%%%%%%%%%%%%%%%%%%%%%%%
80
81 H_ny=A_matrice\(B_matrice*H + C_vektor);
82
83 % % % make sure H does not become negative
84 H_ny(H_ny<0)=0;
85 % % %
86 H=H_ny;
87 %H(1)=H(2); %problem at build up
88 % % % save profiles % % %
89 j_save=j_save+1;
90 D_save(:,j_save)=D;
91 dD_dx_save(2:N-1,j_save)=dD_dx(2:N-1);
92 alpha_save(:,j_save)=alpha;
93 beta_save(:,j_save)=beta;
94 G_save(:,j_save)=G;
95 a_save(:,j_save)=a*(H_star-E(1:N));
96 b_save(:,j_save)=-b*(H_star-E(1:N)).^2;
97 H_save(:,j_save)=H;
98 h_save(:,j_save)=h;
99 H_star_save(:,j_save)=H_star;
100 E_save(:,j_save)=E;
101 H_over_save(j_save)=H_over(1);

```

```

102 end
103
104 Date      %Call programme to date the model

```

A.2 Dating program

```

1 %
2 % Date.m
3 %
4 % Program to date an ice core located close to an ice divide.
5 % Dating is done by a D-J model.
6 % Input files needed:
7 % acc_h.dat [Time(i), acc(i), H(i) , i=1,N]
8 % Time(i) time [years before present]
9 % acc(i) surface accumulation rates [m ice equivalent]
10 % H(i) ice thicknesses in ice equivalent [m]
11 % Made by Dorthe Dahl-Jensen 19-02-97
12 %
13
14 knaek=.2;      % kink-height fraction of H
15 wmelt=0;      % bottom melt (= 0 at FI)
16 FB=0.1;      % bottom fraction of sliding
17 acc=dt*G_save(1,M_start:M)'; %accumulation [m/year]
18 dt=1;
19
20 %matrix with 1. time, 2. acc, 3. height and 4. dH/dt
21 climate=ones(M,4);
22 climate(:,1)=dt*(1:M); % time
23 climate(:,2)=acc; % accumulation
24 climate(:,3)=H_save(1,M_start:M); %Thickness, H
25 climate(2:M-1,4)=(H_save(1,M_start+2:M)-H_save(1,M_start:M-2)).*1.5;
26 climate(1,4)=climate(2,4); %climate(:,4) is dH/dt
27 climate(M,4)=climate(M-1,4);
28
29 %
30 % Set variables for start of time loop
31 %
32
33 Z_array=zeros(M,1);
34 j_array=0;
35 h_knaek=0;
36
37 %
38 % Start time loop
39 %
40 save_nr=400; %save the plot every (save_nr*dt) years
41 fig_nr=0;
42 time_plot=zeros(M,round(M/save_nr));
43
44 for T=M:-dt:dt
45     A=climate(j_array+1,2);
46     H=climate(j_array+1,3);

```

```

47 dHdt=climate(j_array+1,4);
48 h_knaek=knaek*H;
49 R=(A-dHdt)/(H-0.5*h_knaek*(1-FB));
50
51 j_array=j_array+1;
52 Z_array(j_array)=H;
53
54 if mod(j_array,save_nr)==0
55     save_fig
56 end
57
58 %
59 % Move the Nstop layers that are in the ice down for a period of T years
60 %
61 for j=1:j_array
62     Z=Z_array(j);
63     Znew=Tracedown(Z,R,h_knaek,H,FB,wmelt,dt);
64     Z_array(j)=Znew;
65 end
66 end
67 FI_al=[climate(:,1),H-Z_array];

1 function Znew=Tracedown(Z,R,h_knaek,FB,dt)
2 %
3 % Function to calculate the new position of a layer, Znew, after it is
4 % moved down in T years.
5
6 if Z > h_knaek
7     Znew = (Z - (.5*h_knaek)*(1-FB))*exp(-dt*R) + .5*h_knaek*(1-FB);
8 else
9     C = Z/(FB + (.5/h_knaek)*(1 - FB)*Z)*exp(-dt*FB*R);
10    Znew = (FB*C)/(1-(.5/h_knaek)*(1 - FB)*C);
11 end

```

References

- [Andersen et al. 2006] Andersen, K.K., Ditlevsen, P.D., Rasmussen, S.O., Clausen, H.B., Vinther, B.M., Johnsen, S.J. and Steffensen, J.P. (2006). *Retrieving a common accumulation record from Greenland ice cores for the past 1800 years* **Journal of Geophysical Research** Vol 111 12 pp.
- [Anisimov et al. 2007] Anisimov, O., Vaughan, D., Callaghan, T., Furgal, C., Marchant, H., Prowse, T., Vilhjalmsson, H. and Walsh, J. (2007). *Polar regions (Arctic and Antarctic)*, **Climate change 2007: Impacts, adaptation and vulnerability. Contribution of working group ii to the fourth assessment report of the intergovernmental panel on climate change.**
- [Azuma 1994] Azuma, N. (1994). *A flow law for anisotropic ice and its application for ice sheets*, **Earth and Planetary Science Letters** Vol 128 601-614.
- [Boulton et al. 1984] Boulton, G.S., Smith, G.D. and Morland L.W. (1984). *The Reconstruction of Former Ice Sheets and their Mass Balance Characteristics Using a Non-Linearly Viscous Flow Model*, **Journal of Glaciology** Vol. 30 140-150.
- [Brotchie and Silvester 1969] Brotchie, J.F. and Silvester, R. (1969). *On Crustal Flexure* **Journal of Geophysical Research** Vol. 74, 5240-5252.
- [Budd and Radok 1971] Budd, W.F. and Radok, U. (1971). *Glaciers and other large icemasses*, **Reports on Progress in Physics** Vol. 34(1) 1-70.
- [Clausen et al. 1997] Clausen, H.B., Hammer, C.U., Hvidberg, C.S., Dahl-Jensen, D., Steffensen, J.P., Kipfstuhl, J. and Legrand, M. (1997). *A comparison of the volcanic records over the past 4000 years from the Greenland Ice Core Project and Dye 3 Greenland ice cores*, **Journal of Geophysical Research** Vol. 102 26,707-26,723.
- [Clausen et al. 2001] Clausen, H.B., Stampe, M., Hammer, C.U., Hvidberg, C.S., Dahl-Jensen, D. and Steffensen, J.P. (2001). *Glaciological and Chemical Studies on ice Cores from Hans Tausen Iskappe, Greenland*, **Meddelelser om Grønland, Geoscience** **39**, 123-149.
- [Clausen, pers. comm.] Clausen, H. B. (2009). Personal communication.
- [Dahl-Jensen, pers. comm.] Dahl-Jensen, D. (2009). Personal communication.

- [Dahl-Jensen et al. 1993] Dahl-Jensen, D., Johnsen, S.J., Hammer, C.U., Clausen, H.B. and Jouzel, J. (1993) *Past Accumulation rates derived from observed annual layers in the GRIP ice core from Summit, Central Greenland*, **Nato ASI series I 12**, ed. WR. Peltier.
- [Dahl-Jensen et al. 1998] Dahl-Jensen, D., Mosegaard, K., Gundestrup, N., Clow, G.D., Johnsen, S.J., Hansen, A.W. and Balling, N. (1998). *Past Temperatures Directly from the Greenland Ice Sheet*, **Science** Vol. 282, 268-271.
- [Dansgaard 1964] Dansgaard, W. (1964). *Stable isotopes in precipitation*, **Tellus** Vol. 16 436-468.
- [Dansgaard and Johnsen 1969] Dansgaard, W. and Johnsen, S.J. (1969). *A Flow Model and a Time Scale for the Ice Core from Camp Century, Greenland*, **Journal of Glaciology** Vol 8(53) 215-223.
- [Funder and Hansen 1996] Funder, S. and Hansen, L. (1996). *The Greenland ice sheet - a model for its culmination and decay during and after the last glacial maximum*, **Bulletin of the Geological Society of Denmark** Vol 42 137-152.
- [Glen 1955] Glen, J.W. (1955). *The Creep of Polycrystalline Ice*, **Proceedings of the Royal Society of London** Vol. 228 519-538.
- [Hammer 1980] Hammer, C.U. (1980). *Acidity of Polar Ice Cores in Relation to Absolute Dating, Past Volcanism, and Radio Echoes*, **Journal of Glaciology** Vol. 25 359-372.
- [Hammer et al. 1978] Hammer, C.U., Clausen, H.B., Dansgaard, W., Gundestrup, N., Johnsen, S.J. and Reeh, N. (1978). *Dating of Greenland Ice Cores by Flow Models, Isotopes, Volcanic Debris and Continental Dust.*, **Journal of Glaciology** Vol. 20, 3-26.
- [Hammer et al. 2001] Hammer, C.U., Johnsen, S.J., Clausen, H.B., Dahl-Jensen, D., Gundestrup, N. and Steffensen, J.P. (2001). *The Paleoclimatic Record from a 345 m long Ice Core from the Hans Tausen Iskappe.*, **Meddelelser om Grønland**, Geoscience **39**, 87-95.
- [Hooke 2005] Hooke, R.Leb. (2005). *Principles of glacier mechanics, 2. ed.*, Cambridge University Press.
- [Johnsen et al. 1992] Johnsen, S.J., Clausen, H.B., Dansgaard, W., Gundestrup, N.S., Hansson, M., Jonsson, P., Steffensen, J.P. and Sveinbjörnsdóttir, A.E (1992). *A "deep" icecore from East Greenland.*, **Meddelelser om Grønland**, Geoscience **29**, 1-22.
- [Johnsen et al. 1995] Johnsen, S.J., Dahl-Jensen, D., Dansgaard, W. and Gundestrup, N. (1995). *Greenland temperatures derived from GRIP*

- borehole temperatures and ice core isotope profiles, **Tellus** Vol 47B 624-629.
- [Johnsen et al. 1997] Johnsen, S.J. and 14 others (1997). *The $\delta^{18}\text{O}$ record along the Greenland Ice Core Project deep ice core and the problem of possible Eemian climatic instability*, **Journal of Geophysical Research**, (102) 26,397-26,410.
- [Koerner 1977] Koerner, R.M. (1977). *Devon Island Ice Cap: Core Stratigraphy and Paleoclimate*, **Science** Vol. 196 15-18.
- [Koerner and Fisher 1990] Koerner, R.M. and Fisher, D. (1990). *A record of Holocene summer climate from a Canadian high-Arctic ice core*, **Nature** Vol. 343 630-631.
- [Koerner and Fisher 2002] Koerner, R.M and Fisher, D. (2002). *Ice-core evidence for widespread Arctic glacier retreat in the Last Interglacial and the early Holocene*, **Annals of Glaciology** Vol. 35 19â24.
- [Krabill et al. 2000] Krabill, W., Abdalati, W., Frederick, E., Manizade, S., Martin, C., Sonntag, J., Swift, R., Thomas, R., Wright, W. and Yungel, J. (2000). *Greenland Ice Sheet: High-elevation balance and peripheral thinning.*, **Science** Vol. 289 428-430.
- [Lautrup 2005] Lautrup, B. (2005). *Physics of Continuous Matter*, IOP Publishing.
- [Madsen 1997] Madsen, K.N. (1997). *Hans Tausen iskernen - studier af krystalstruktur, datering og smeltelagsstratigrafi*, Master Thesis: Niels Bohr Institute, Copenhagen University.
- [Meese et al. 1997] Meese, D.A. and 8 others (1997). *The Greenland Ice Sheet Project 2 depth-age scale: Methods and results* **Journal of Geophysical Research** Vol. 102 26,411-26,423.
- [Meier et al. 2007] Meier, M., Dyurgerov, M., Rick, U., OâNeel, S., Pfeffer, W., Anderson, R., Anderson, S. and Glazovsky, A. (2007). *Glaciers Dominate Eustatic Sea-Level Rise in the 21st Century*, **Science** Vol. 317 1064â1067.
- [NGRIP members 2004] NGRIP members (2004). *High-resolution record of Northern Hemisphere climate extending into the last interglacial period*, **Nature** Vol. 431 147-151.
- [Nye 1957] Nye, J.F. (1957). *The Distribution of Stress and Velocity in Glaciers and Ice-Sheets*, **Proceedings of the Royal Society of London**, Vol.239 113-133.
- [Oerlemans 1980] Oerlemans, J. (1980). *Model experiments on the 100,000-yr glacial cycle*, **Nature** Vol. 287, 430-432.

- [Oerlemans 1981] Oerlemans, J. (1981). *Some basic experiments with a vertically-integrated ice sheet model*, **Tellus** 33, 1-11.
- [Oerlemans 2008] Oerlemans, J. (2008). *Minimal Glacier Models*, Igitur, Universiteitsbibliotheek Utrecht.
- [Overpeck et al. 1997] Overpeck, J. and 17 others (1997). *Arctic Environmental Change of the Last Four Centuries*, **Science** Vol. 278 1251-1256.
- [Paren and Robin 1975] Paren, J.G. and Robin, G. de Q. (1975). *Internal reflections in polar ice sheets*. **Journal of Glaciology** Vol. 14(71) 251-259.
- [Paterson 1994] Paterson, W.S.B. (1994). *The Physics of Glaciers, 3. ed.*, Butterworth-Heinemann.
- [Petrenko and Whitworth 1999] Petrenko, V.F. and Whitworth, R.W. (1999). *Physics of Ice*, Oxford University Press.
- [Press et al. 2003] Press, W., Teukolsky, S., Wetterling, W. and Flannery, B. (2003). *Numerical Recipes in FORTRAN 77* **Cambridge University Press**.
- [Pritchard et al. 2009] Pritchard, H.D., Arthern, R.J., Vaughan, D.G and Edwards, L.A. (2009). *Extensive dynamic thinning on the margins of the Greenland and Antarctic ice sheets* **Nature** Vol. 461 971-975.
- [Rasmussen 2004] Rasmussen, L. (2004). *Set fra oven: Et hjørne af Grønland*, **Vejret** Vol. 100 17-20.
- [Reeh et al. 2001] Reeh, N., Olesen, O.B., Thomsen, H.H., Starzer, W. and Bøggild, C.E. (2001). *Mass balance parameterisation for Hans Tausen Iskappe, Peary Land, North Greenland*, **Meddelelser om Grønland, Geoscience** 39, 57-69.
- [Reeh et al. 2002] Reeh, N., Oerter, H. and Thomsen, H.H. (2002). *Comparison between Greenland ice-margin and ice-core oxygen-18 records*, **Annals of Glaciology** Vol. 35 136-144.
- [Rinne pers. comm.] Rinne, E. (2010). Personal communication.
- [Skinner and Porter 1987] Skinner, B.J. and Porter, S.C. (1987). *Physical Geology*, **John Wiley and sons**.
- [Steffensen 1988] Steffensen, J.P. (1988). *Analysis of the Seasonal Variation in Dust, Cl^- , NO_3^- and SO_4^{2-} in two Central Greenland Firn Cores*, **Annals of Glaciology** Vol. 10 171-177.
- [Steffensen 2005] Steffensen, J.P. (2005). *Appendix on Flade Isblink, personal distribution*

- [Steffensen pers. comm.] Steffensen, J.P. (2009). Personal communication.
- [Svensson et al. 2008] Svensson, A. and 13 others (2008). *A 60 000 year Greenland stratigraphic chronology*, **Climate of the Past** 4, 47-57.
- [Vinther et al. 2008] Vinther, B.M., Clausen, H.B., Fisher, D.A., Koerner, R.M., Johnsen, S.J., Andersen, K.K., Dahl-Jensen, D., Rasmussen, S.O., Steffensen, J.P. and Svensson, A.M. (2008). *Synchronizing ice cores from the Renland and Agassiz ice caps to the Greenland Ice Core Chronology*, **Journal of Geophysical Research** Vol. 113 D08115
- [Weertman 1961] Weertman, J. (1961) *Stability of ice-age ice sheets*, **Journal of Geophysical Research** Vol. 66(11) 3783-3792.